Discovery and Optimization of Pyrimidone Indoline Amide PI3Kß Inhibitors for the Treatment of Phosphatase and TENsin homologue (PTEN)-Deficient Cancers.

ARTICLE *in* JOURNAL OF MEDICINAL CHEMISTRY · JANUARY 2014

Impact Factor: 5.45 · DOI: 10.1021/jm401642q · Source: PubMed

Journal of Medicinal Chemistry

Article

pubs.acs.org/jmc

Discovery and Optimization of Pyrimidone Indoline Amide PI3Kβ Inhibitors for the Treatment of Phosphatase and Tensin Homologue (PTEN)-Deficient Cancers

Victor Certal,[‡] Jean-Christophe Carry,[‡] Frank Halley,*[,‡] Angela Virone-Oddos,[‡] Fabienne Thompson,[‡] Bruno Filoche-Rommé,[‡] Youssef El-Ahmad,[‡] Andreas Karlsson,[§] Véronique Charrier,[‡] Cécile Delorme,[‡] Alexey Rak,[§] Pierre-Yves Abecassis,[#] Céline Amara,[#] Loïc Vincent,[‡] Hélène Bonnevaux,[‡] Jean-Paul Nicolas,[‡] Magali Mathieu,[§] Thomas Bertrand,[§] Jean-Pierre Marquette,[§] Nadine Michot,[†] Tsiala Benard,[⊥] Marc-Antoine Perrin,[∥] Olivier Lemaitre,[‡] Stephane Guerif,[‡] Sébastien Perron,[‡] Sylvie Monget,[‡] Florence Gruss-Leleu,[‡] Gilles Doerflinger,[‡] Houlfa Guizani,[‡] Maurice Brollo,[‡] Laurence Delbarre,[‡] Luc Bertin,[‡] Patrick Richepin,[‡] Véronique Loyau,[‡] Carlos Garcia-Echeverria,[‡] Christoph Lengauer,[‡] and Laurent Schio[‡]

[‡]Oncology Drug Discovery, [§]Structure Design Informatics, and Structural Biology, [#]Drug Disposition and Safety (DSAR), [†]Protein Production,[⊥]Pharmaceutical Sciences, [∥]Analytical Sciences, Sanofi, 13, quai Jules Guesde, 94403 Vitry-sur-Seine, France

ABSTRACT: Compelling molecular biology publications have reported the implication of phosphoinositide kinase PI3Kβ in PTEN-deficient cell line growth and proliferation. These findings supported a scientific rationale for the development of PI3Kβ-specific inhibitors for the treatment of PTEN-deficient cancers. This paper describes the discovery of 2-[2-(2,3-dihydro-indol-1-yl)-2-oxo-ethyl]-6-morpholin-4-yl-3*H*-pyrimidin-4-one (**7**) and the optimization of this new series of active and selective pyrimidone indoline amide PI3Kβ inhibitors. 2-[2-(2-Methyl-2,3-dihydro-indol-1-yl)-2-oxo-ethyl]-6-morpholin-4-yl-3*H*-pyrimidin-4-one (**28**), identified following a carefully designed methyl scan, displayed improved physicochemical and *in vitro* pharmacokinetic properties. Structural biology efforts enabled the acquisition of the first X-ray cocrystal structure of p110β with the selective inhibitor compound **28** bound to the ATP site. The nonplanar binding mode described herein is consistent with observed structure−activity relationship for the series. Compound **28** demonstrated significant *in vivo* activity in a UACC-62 xenograft model in mice, warranting further preclinical investigation. Following successful development, compound **28** entered phase I/Ib clinical trial in patients with advanced cancer.

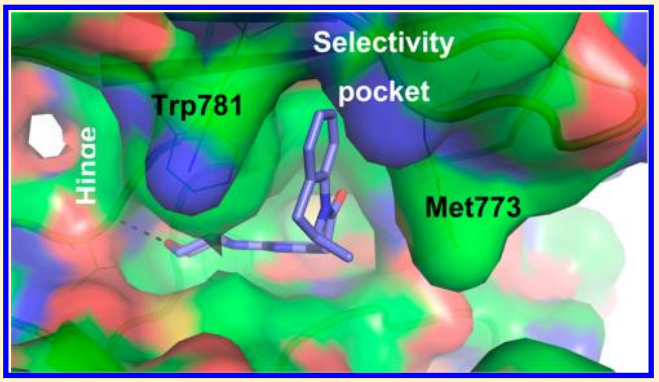

INTRODUCTION

The phosphoinositide 3-kinase (PI3K) family of phospholipid kinases is divided into three classes (I, II, and III), based on structural characteristics and substrate preferences.[1] Class II and class III phospholipid kinases are composed, respectively, of PI3KC2α, PI3KC2β, and PI3KC2γ and PIK3C3 also known as VPS34.[1] The closest kinase analogues in terms of sequence evolution are the class IV PI3K-related protein kinases known as ataxia telangiectasia mutated (ATM), ataxia telangiectasia and Rad3 related (ATR), mammalian target of rapamycin (mTOR) and DNA-dependent protein kinase (DNA-PK).[2]

The best characterized class I PI3Ks phosphorylate the phosphatidylinositol-4,5-bisphosphate (PIP2) on the 3-position to yield the second messenger phosphatidylinositol-3,4,5-trisphosphate (PIP3), which activates the downstream Akt pathway.[3] Class I is further classified into class IA, including PI3Kα, β, and δ, activated by RTKs, G-protein-coupled receptors (GPCRs), and rat sarcoma (RAS), and class IB, consisting of PI3Kγ, regulated exclusively by GPCRs.[3] Class IA PI3K involved in human cancers are heterodimer enzymes composed of a p85 regulatory subunit and a p110 catalytic subunit harboring the kinase domain.[4] The p110α, β, and δ subunits are encoded by *PIK3CA*, *PIK3CB*, and *PIK3CD* genes, respectively.[1]

PIP3 recruits phosphoinositide-dependent kinase-1 (PDK1) and protein kinase B (PKB or Akt) to the cell membrane through binding to pleckstrin homology (PH) domain, bringing both kinases in close proximity. PDK1 phosphorylates first Akt on Thr308 followed by mTORC2 on Ser473 leading to full Akt activation and upregulation of downstream effectors triggering cell growth and survival.[3−5]

Received: October 23, 2013
Published: January 4, 2014

   dx.doi.org/10.1021/jm401642q | *J. Med. Chem.* 2014, 57, 903−920

Abnormal PI3K pathway activation plays a major role in cancer, either as a result of RTK activation or somatic mutations of major components of the pathway, including activating point mutations and amplification of the *PIK3CA* gene, as well as loss of negative regulatory proteins such as phosphatase and tensin homologue (PTEN). Most of the PI3K inhibitors currently in clinical development inhibit all class I PI3K isoforms. However, several recent reports support the clinical development of isoform-specific inhibitors.[6,7]

While PI3Kα specific inhibitors are predicted to inhibit growth of tumors with *PIK3CA* mutations, PTEN-deficient tumors have been shown to depend on PI3Kβ activity.[8,9] Furthermore, isoform-specific PI3K inhibitors may exhibit improved safety profiles compared with pan-PI3K inhibitors and pending structure-related pharmacological properties could be combined with other targeted therapies or standard of care agents. In recent years, few publications have emerged describing the identification of new PI3Kβ inhibitors to treat PTEN-deficient cancers, obtained from a pharmacophore-directed design[10] or TGX-221 rescaffolding.[11−16] This paper describes the discovery of PI3Kβ selective small molecular mass pyrimidone indoline amide inhibitors and their optimization toward a clinical candidate. Especially, emphasis has been directed at solubility improvement through a methyl scan approach based on crystal packing disruption. Herein is disclosed the X-ray structure of the candidate compound bound to PI3Kβ at 2.8 Å resolution and its characterization in PTEN-deficient *in vitro* and *in vivo* tumor cell models.

LEAD DISCOVERY AND OPTIMIZATION

Compound **5**[17] (Figure 1) was identified following a high throughput screening, and the investigation and limitation of

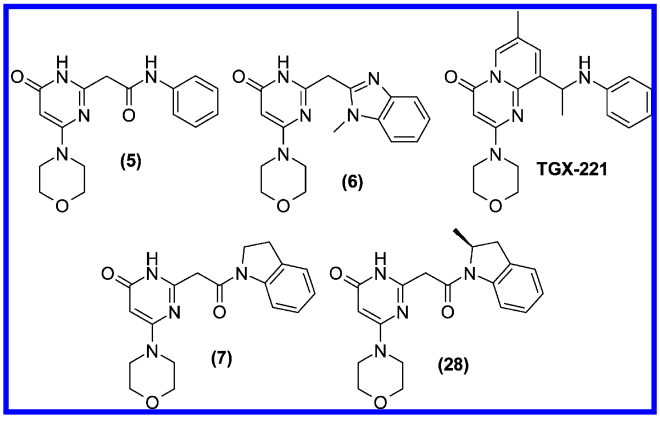

Figure 1. Structures of representative examples of PI3Kβ inhibitors.

close anilide analogues was reported in a recent publication.[18] Optimization of benzimidazole and benzoxazole derivatives was previously published, and compound **6** was used as a tool compound for *in vivo* efficacy studies in a PTEN-deleted PC3 xenograft mice model.[19] During the optimization phase of compound **5**, aniline replacement by secondary amines was investigated, and the indoline amide **7** displayed very potent inhibition of PI3Kβ (IC_{50} = 460 nM, 4 nM, 28 nM, and >10 μM on PI3Kα, β, δ, and γ, respectively), with a high LE[20] = 0.46 for PI3Kβ. With this promising result in hand, a thorough investigation of indoline substitutions was initiated in order to identify a compound with drug-like properties.

To guide program optimization, compound **7** was docked in a PI3Kβ homology model, built from publicly available structures as described in a previous publication[19] (See Figure 2).

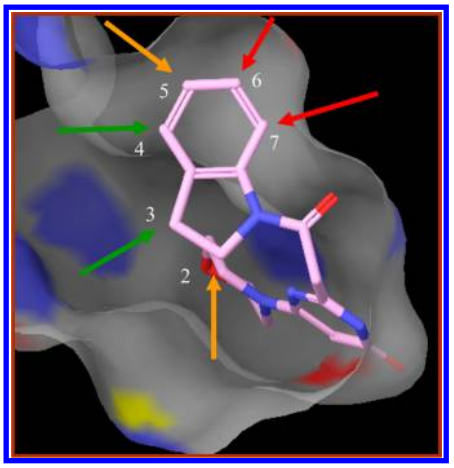

Figure 2. Proposed binding of pyrimidone indoline amide **7** in PI3Kβ showing the favorable (green arrows, positions 3 and 4), tolerated (orange arrows, positions 2 and 5), and detrimental (red arrows, positions 6 and 7) sites for substitution on the indoline. Tools in the Schrödinger molecular modeling suite (Maestro, version 9.0; Schrödinger, LLC, New York, NY, 2007) were used to create homology models (Prime) of PI3Kβ, prepare ligands (LigPrep), and perform ligand docking and scoring (Glide). PDB access codes for template structures used in homology modeling: 4G11 and 2WXF.

Cellular Akt phosphorylation was determined in PTEN-deleted PC3 prostate cancer cell line, measuring pAkt-S473 inhibition. Table 1 shows the biochemical and cellular activities obtained with the reference compounds (TGX-221[21] and **6**)[19] and the different substituted pyrimidone indoline amides, compounds **7**−**29**. All these compounds displayed IC_{50} on mTOR above 10 μM (data not shown).

Docking of this series in the ATP pocket of the PI3Kβ homology model predicted steric hindrance at aryl positions C-6 and C-7 of the indoline (Figure 2) and chemical modification focused at C-5 and mainly at C-4. Position C-5 tolerated only small groups such as fluorine (compound **8**). Introduction of a chlorine (compound **9**) resulted in a 20-fold decrease in activity. As suggested by modeling, C-4 was more amenable to various substitutions. Introduction of halogens such as fluorine (compound **10**), chlorine (compound **11**), and bromine (compound **12**) led to the most potent compounds with activity reaching 1 nM in biochemical (compound **11**) or cellular (compound **12**) assays. Introduction of a methyl (compound **13**), provided a binding activity comparable to compound **10**, and replacement with a more electron-donating methoxy group (compound **14**) or an electron-withdrawing group such as trifuoromethyl (compound **15**) did not improve inhibitory activity. Introduction of the OCF_3 group (compound **16**), which has both electron-withdrawing ability and lipophilicity close to a halogen,[22] did not improve activity. To investigate further the space available at this position, a phenyl (compound **17**) was introduced, which retained most of the activity, and thus, heterocycles were investigated to modulate physicochemical properties. To improve solubility, the *ortho*-, *meta*-, and *para*-pyridines (compounds **18**, **19**, and **20**, respectively) were introduced, and all retained some biochemical activity, but the most active *para*-pyridine lost almost 10-fold cellular potency.

dx.doi.org/10.1021/jm401642q | J. Med. Chem. 2014, 57, 903−920

Table 1. Biochemical and Cellular Activity of Reference Compound TGX-221, Benzimidazole 6, and Pyrimidone Indoline Amides 7−29

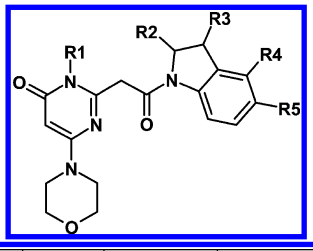

Compd	R1	R2	R3	R4	R5	MW	PI3Kα[a] IC_{50} (nM)	PI3Kβ[a] IC_{50} (nM)	PI3Kδ[a] IC_{50} (nM)	PI3Kγ[a] IC_{50} (nM)	pAkt[a,b] IC_{50} (nM)	Solubility at pH7.4 (μM)
TGX-221	-	-	-	-	-	364	10000	30	851	10000	10	-
6	-	-	-	-	-	325	10000	99	1395	10000	76	
7	H	H	H	H	H	340	460	4	28	10000	15	12
8	H	H	H	H	F	358	426	4	17	1590	7	31
9	H	H	H	H	Cl	375	2020	79	4135	10000	124	3
10	H	H	H	F	H	358	2450	6	122	6215	5	14
11	H	H	H	Cl	H	375	86	1	21	1131	3	5
12	H	H	H	Br	H	419	85	6	55	3975	1	2
13	H	H	H	Me	H	354	138	5	24	1780	3	3
14	H	H	H	OMe	H	370	2425	41	648	10000	60	5
15	H	H	H	CF_3	H	408	390	10	98	8400	9	12
16	H	H	H	OCF_3	H	424	1000	33	34	7418	54	12
17	H	H	H	Ph	H	416	217	8	18	1532	24	-
18	H	H	H	o-Py	H	417	2375	98	106	8966	66	110
19	H	H	H	m-Py	H	417	361	17	7	2461	53	60
20	H	H	H	p-Py	H	417	1000	10	22	1000	94	69
21	H	H	H	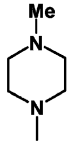	H	439	960	407	22	10000	167	1496
22	H	H	H	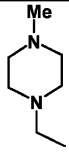	H	453	660	332	2	10000	272	4419

dx.doi.org/10.1021/jm401642q | J. Med. Chem. 2014, 57, 903−920

Table 1. continued

Compd	R1	R2	R3	R4	R5	MW	PI3Kα[a] IC_{50} (nM)	PI3Kβ[a] IC_{50} (nM)	PI3Kδ[a] IC_{50} (nM)	PI3Kγ[a] IC_{50} (nM)	pAkt[a,b] IC_{50} (nM)	Solubility at pH7.4 (μM)
23	Me	H	H	H	H	354	4320	48	278	10000	20	36
24	H	Me[c]	H	H	H	354	322	4	36	9149	6	2754
25	H	Di-Me	H	H	H	368	10000	102	580	10000	78	46
26	H	H	Me[c]	H	H	354	2265	22	87	10000	13	3
27	H	H	Di-Me	H	H	368	5421	17	278	10000	28	46
28	H	(S)-Me	H	H	H	354	1539	23	468	10000	49	928
29	H	(R)-Me	H	H	H	354	569	6	6	3315	12	2497

[a] IC_{50} values are reported as the mean from at least two independent experiments. See Experimental Methods for assay details. [b] pAkt-S473 inhibition in PC3 cell line. [c] Compounds **24** and **26** are racemates.

Further substitution with six-membered aliphatic heterocycles such as the directly linked methylpiperidine (compound **21**) or branched methylpiperidine (compound **22**) led to a 40-fold loss of PI3K*β* activity and to a gain of up to 9-fold in PI3K*δ* activity compared with compound **17**. The reverse selectivity observed for compounds **21** and especially **22** (>100-fold selectivity in favor of PI3K*δ*) is most likely due to the presence of a lysine (Lys771) in the P-loop of PI3K*β*, replacing a threonine (Thr750) at the equivalent position in PI3K*δ*. This lysine or threonine residue is located close to the substituent at C-4 of the indoline moiety of the bound inhibitor. The small threonine side chain in PI3K*δ* would allow binding of the bulky and positively charged moieties in compounds **21** and **22**, while the large and positively charged lysine side chain in PI3K*β* would be detrimental to binding. This observation was general for all solubilizing amines introduced at that position, and other approaches to improve solubility were sought.

One physicochemical limitation identified within this series was the poor aqueous solubility[23] of the core scaffold exemplified with compound **7** (Table 1), leading to major formulation issues. Considering the low molecular mass and cLogP of these compounds, strong crystal packing with intermolecular hydrogen bonding was suspected to contribute to the observed limited aqueous solubility. The high melting point measured for compound **7** (mp 285 °C) was in agreement with this working hypothesis.[24]

The X-ray crystal structure of compound **7** was solved from single diffraction data. Crystal packing analysis shows a rich intermolecular interaction pattern; this results in an energetically strong crystal packing as reflected by the high melting point. Indeed pairs of centrosymmetrically related molecules form strong planar hydrogen-bonded dimers through donor−acceptor N−H···O contacts of 2.74 Å between pyrimidone moieties. Closely interconnected both by indoline *π*-stacking and indoline/morpholine C−H···*π* interactions, dimers form layers parallel to the {101} plane (see Figure 3). Finally to build the three-dimensional structure of the crystal, {101} close-packed layers are staggered to maximize van der Waals interactions mainly between indoline and also morpholine moieties.

Crystallographic study of compound **7** confirmed a strong *π*−*π* interaction between the indoline rings and an extended network of head-to-tail hydrogen bonding (Figure 3). It was postulated that improved water solubility could be obtained through disruption of the crystal packing via the introduction of a methyl group[25] at positions selected according to the model (Figure 2). This limited methyl scan was performed at position R1 (see Table 1) to break the hydrogen bond network and at positions R2 and R3 to prevent *π*−*π* hydrophobic interactions.

Compared with compound **7**, it was found that the introduction of a *N*-methyl on the pyrimidone ring at position R1 (compound **23**) had a limited effect on solubility (achieving only a 3-fold increase) whereas activity dropped by 10-fold (Table 1). This result is similar to the one previously reported for the benzimidazole series.[19] This drop in potency suggested that polar groups interacting with the residues Asp931 or Lys799 in PI3K*β* would be preferred at this position. Mono methyl substitution at position R2 (compound **24**) led to a remarkable 100-fold gain in solubility while retaining activity. The achiral gem-dimethyl substitution (compound **25**) led to a disappointing 4-fold gain in solubility and to a 25-fold loss in activity. At position R3, the mono methyl (compound **26**) had no effect on solubility compared with compound **7**, while the achiral gem-dimethyl (compound **27**) showed a modest 4-fold increase,

dx.doi.org/10.1021/jm401642q | J. Med. Chem. 2014, 57, 903−920

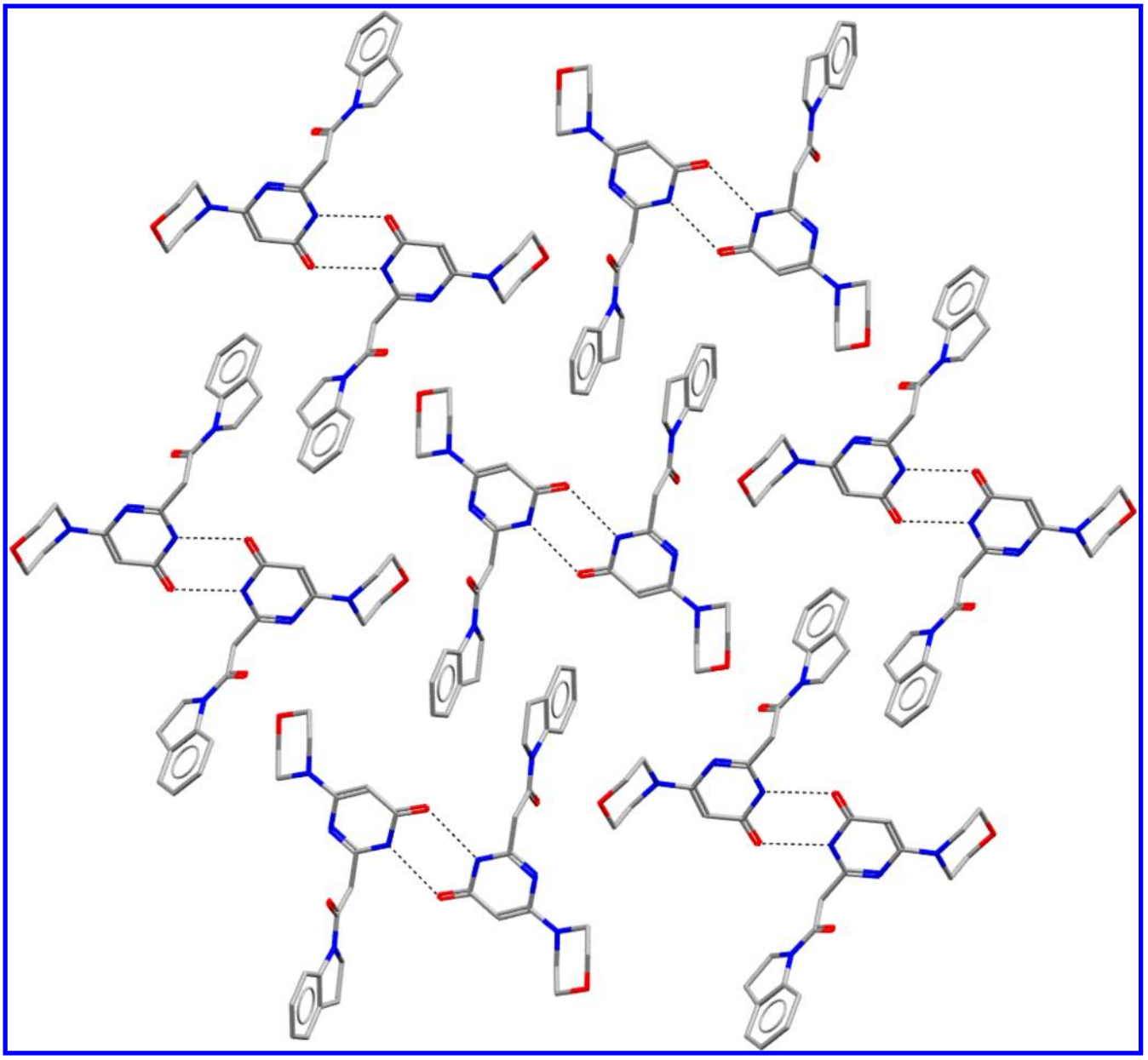

Figure 3. Crystal structure of compound **7**. The {101} compound **7** dimer layer showing a rich and energetically strong intermolecular interaction pattern: H-bonding cyclic dimer, π-stacking, and C−H···π interactions (carbon atom, gray; nitrogen atom, blue; oxygen atom, red; hydrogen atoms are omitted for clarity). See Table 8 for crystal data, structure refinement, and CCDC code.

both compounds displaying similar biological activities. Owing to structure related promising solubility, racemic compound **24** was separated into its two enantiomers. The (*R*)-isomer (**29**) retained the full PI3Kβ activity at the expense of the PI3Kδ selectivity, whereas the (*S*)-isomer (**28**) lost some activity on PI3Kβ but retained selectivity toward PI3Kδ. The solubilities observed for the racemic compound **24** and the enantiomers **28** and **29** are in a range of a factor 3.[26] The improved solubility of compound **28** (928 μM) compared with compound **7** (12 μM) could be explained by a drastic change in intermolecular interaction. Following this encouraging result, the 2-methyl was introduced on the indoline of all potent compounds to improve solubility; this resulted in, as expected, the identification of new potent and soluble compounds, but all presented metabolic issues and none were further developed.

Confirmation of compound **28**'s absolute configuration was attributed from synthesis via (*S*)-2-methyl indoline coupling (results not shown) and crystallographic studies in complex with PI3Kβ (see Figure 6).

When biochemical PI3Kβ activities and cellular pAkt-S473 inhibition potencies were compared in Table 1, there appeared to be an overall consistency in data relationship. Plotting the biochemical activity on PI3Kβ (pIC_{50}) against the cellular potency on pAkt (pIC_{50}), a trend for correlation (r^2 = 0.674, see Figure 4) was observed suggesting an overall acceptable cellular permeability.

The *in vitro* ADME properties of a selected number of compounds (PI3Kβ IC_{50} < 100 nM) was further investigated (Table 2).

All selected compounds had molecular mass below 450 and ClogP below 3; polar surface area (PSA) was below 140 Å^2. Permeability measurements in CaCo2 cell line TC7 clone[27] were found to be variable and uncorrelated to PSA or cLogP.[28] For example, compounds **9** and **11**, differing only by the position of the chlorine atom and hence having identical mass

dx.doi.org/10.1021/jm401642q | J. Med. Chem. 2014, 57, 903−920

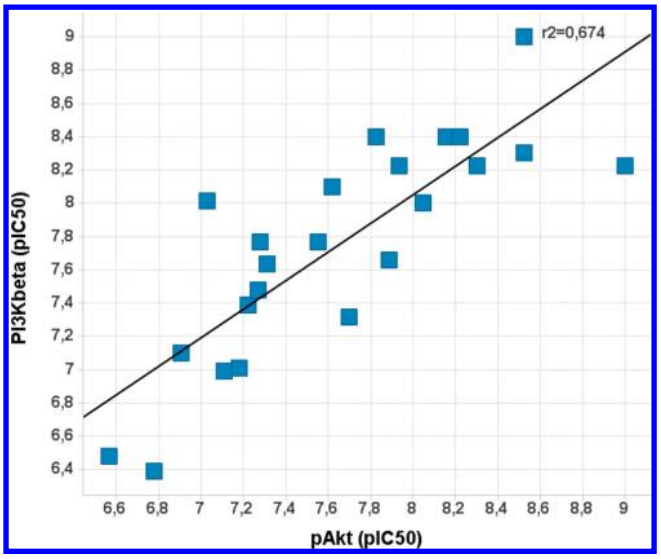

Figure 4. PI3Kβ biochemistry pIC_{50} and pAkt-S473 cellular pIC_{50} correlation for compounds **7**–**29**.

and PSA and similar cLogP, presented a 6-fold ratio in permeability. It is noteworthy to mention that compound **23** had superior permeability to compound **7**, which was general for most *N*-methyl pyrimidones synthesized (results not shown), in agreement with the general rule of thumb stipulating that minimizing hydrogen bond counts is beneficial for permeability.[29] Further transport assessment in both apical to basolateral (A-B) and basolateral to apical (B-A) directions across the cell monolayer enabled the determination of the efflux ratio, which was found to be higher (>10) for most of the N-H pyrimidones and lower (<5) for the N-Me pyrimidones. Overall it was observed that restricted permeability was linked to efflux activity, most likely due to P-gp. For pyridine compounds **19** and **20**, low permeability was attributed to a high efflux, since log *D* and pK_a values were 1.99 and in the range of 4.5–4.7, respectively, in agreement with potentially high intrinsic passive permeability.[30,31] Metabolic lability was low for unsubstituted or halogenated indoline but higher when substituted with alkyl, alkoxy, or aryl groups. Surprisingly, although the CF_3 derivative **15** displayed the expected protecting effect compared with the methyl analogue **13**, the OCF_3 derivative **16** lacked the anticipated effect over the methoxy analogue **14** on human liver microsomes, being even worse than the chloro derivative **11** on mouse liver microsomes.[22] As illustrated in the "heat map" type representation (Figure 5), all selected compounds had good on target modulation activities. Aqueous solubility was limited for most of the compounds, but permeability on the other hand was generally acceptable.

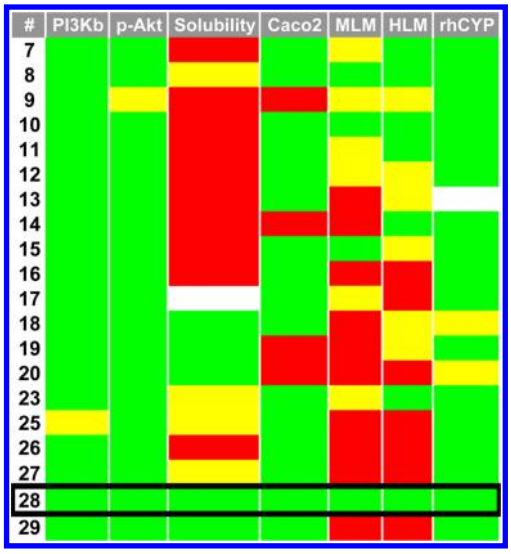

Figure 5. "Heat map" type representation of Table 2 properties with drug-like selected thresholds: IC_{50} < 100 nM, solubility > 50 μM, Caco2 > 20 ms^{-1}, HLM and MLM < 40%, rhCYP > 10 μM (color coding: green = pass; red = fail; yellow = borderline).

Table 2. In Vitro and Calculated Properties of Active Compounds 7–20, 23, and 26–29

compd	MW	PI3Kβ IC_{50} (nM)	pAkt[a] IC_{50} (nM)	cLogP	PSA (Å^2)	solubility, pH 7.4 (μM)	CaCo2 Papp (nm/s)	MLM[b] % lability	HLM[c] % lability	rhCYP3A4[d] IC_{50} (μM)
7	340	4	15	1.2	74	12	59	21	12	40
8	358	4	7	1.2	74	31	30	14	18	40
9	375	79	124	1.2	74	3	14	36	34	40
10	358	6	5	0.6	74	14	54	9	19	40
11	375	1	3	1.6	74	5	88	27	18	40
12	419	6	1	2.1	74	2	42	22	24	40
13	354	5	3	1.5	74	3	74	60	32	
14	370	41	60	1.6	83	5	6	70	0	40
15	408	10	9	2.6	74	12	46	13	24	40
16	424	33	54	2.7	83	12	41	44	48	40
17	416	8	24	3.2	74		71	25	40	40
18	417	98	66	2.0	87	110	42	40	36	11
19	417	17	53	1.9	87	60	8	49	29	40
20	417	10	94	1.8	87	69	4	44	43	31
23	354	48	20	1.1	65	36	83	37	14	40
26	354	22	13	1.7	74	3	75	40	47	40
27	368	17	28	1.1	74	46	40	87	83	40
28	354	23	49	1.5	74	928	48	19	12	40
29	354	6	12	1.7	74		51	52	43	40

[a]pAkt-S473 inhibition in PC3 cell line. [b]MLM = mouse liver microsome. [c]HLM = human liver microsome. Compound was incubated for 20 min at the concentration of 5 μM using a protein concentration of 1 mg/mL. [d]Recombinant human CYP3A4.

dx.doi.org/10.1021/jm401642q | J. Med. Chem. 2014, 57, 903–920

Human and mouse liver microsome stability values were below expectations for most of the compounds, but none had significant rhCYP3A4 inhibitory activity. From this color chart of *in vitro* properties, simple visualization identified compound **28** as a stand alone.

On the basis of its physicochemical and *in vitro* phamacokinetic properties, compound **28** was selected for further investigation.

The protein kinase selectivity profile of this compound was assessed in house against a panel of 192 kinases using a Caliper-based platform,[32] and compound **28** was found inactive up to 10 μM on all protein kinases tested. Similarly, the compound was found to be inactive against mTOR up to 10 μM and moderately active (see Table 3) in DNA-PK biochemical assay.

Table 3. Selectivity of Compound 28 on Different Phospholipid Kinases[a]

mTOR	DNA-PK	PI3KC2α	PI3KC2β	PI3KC2γ	VPS34
>10000	2000	>10000	>1000	3812	183

[a]IC_{50} values in nM are reported as the mean from at least two independent experiments.

The biological activity observed on VPS34 did not translate in a cellular assay (IC_{50} > 10 μM, data not shown).

X-ray Crystal Structure of Compound 28 Bound to PI3Kβ. As a result of extensive efforts in construct design, protein expression, and crystallization, diffracting crystals were successfully obtained of an N-terminal, adaptor binding domain (ABD) truncated version of mouse p110β (residues 114−1064). Here is reported for the first time the X-ray structure at 2.8 Å of p110β in complex with compound **28**, bound to the ATP binding site (Figure 6). The overall structure of p110β is similar (root-mean-square deviation (rmsd) 1.60 Å for backbone atoms of 114−1064) to the previously published full length structure of p110β[33] (pdb code 2Y3A), with exceptions for parts of the C2 domain responsible for binding the iSH2 domain of the regulatory subunit (which is absent in our construct) as well as a few important structural differences in the vicinity of the bound ligand that will be further described below. The structure reveals an inhibitor binding mode that is in good agreement with the binding mode hypothesis used for pyrimidone optimization. The morpholine and pyrimidinone moieties bind in a very similar manner to what has previously been reported for inhibitors in this structural class[18,19,34] in complex with PI3Kγ and PI3Kδ. The morpholine binds to the hinge region via the main-chain nitrogen of Val848, and the pyrimidone occupies a central hydrophobic region of the ATP binding site, sandwiched between Ile797 and Ile930. A water molecule mediates a hydrogen bond from the pyrimidinone carbonyl oxygen to Tyr833 at the back of the ATP pocket on one side and another hydrogen bond to Asp807 in the C-helix. The overall conformation of the P-loop, and in particular, the side chains of Met773 and Trp781 are different from the previously published PI3Kβ structure. Both Met773 and Trp781 are observed in conformations similar to what has previously been described for binding of propeller shaped PI3Kβ and PI3Kδ selective compounds to class I PI3Ks.[36−38] In our structure, the Trp781 side chain is flipped and rotated relative to residue orientation in 2Y3A[33] and adopts a conformation similar to all other X-ray structures of class I PI3Ks. The Met773 side chain is pointed away from Trp781, creating a pocket where the indoline moiety of compound **28** binds, stacking against the indolyl of Trp781 (Figure 6). The Cβ−ε atoms of the Lys771 side chain are creating a hydrophobic surface that forms a continuation of the pocket between Trp781 and Met773, extending to partly cover the 4-position of the indoline in compound **28**. Docking of compound **28** in the PI3Kδ structure showed that the pocket in PI3Kδ does not cover the indoline to the same extent as in PI3Kβ since the

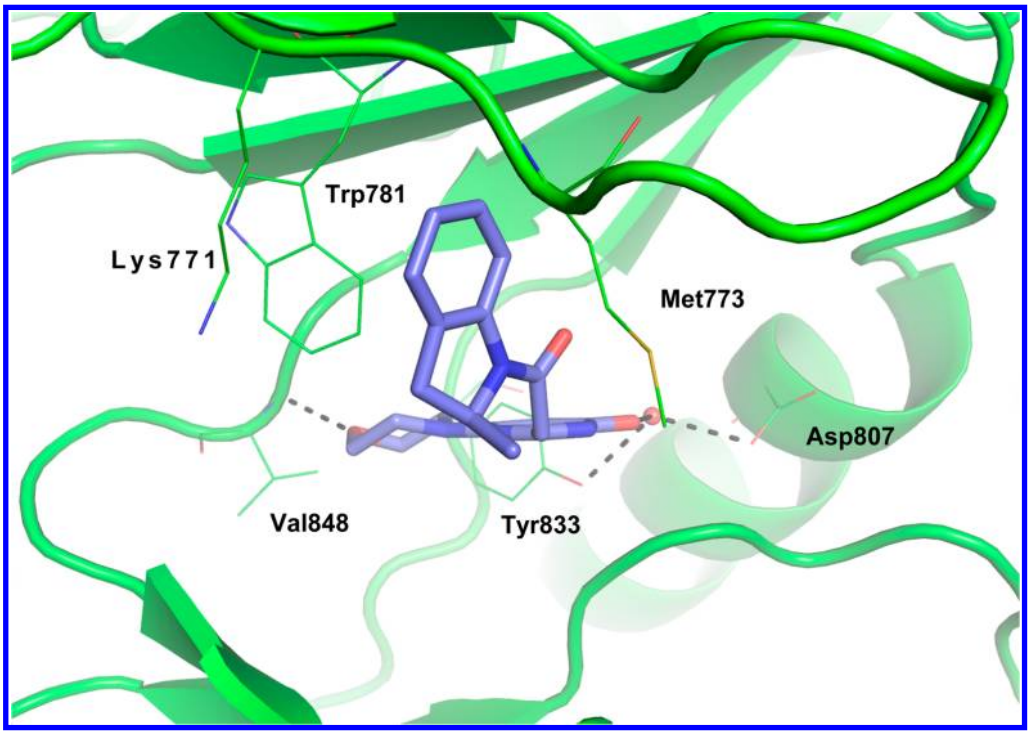

Figure 6. Binding of compound **28** to the ATP binding site of p110β. See Table 9 for X-ray data collection and refinement, pdb 4BFR.

dx.doi.org/10.1021/jm401642q | J. Med. Chem. 2014, 57, 903−920

Table 4. Pharmacokinetic Plasma Parameters of Compound 28 in Female SCID Mice[a]

route	dose (mg/kg)	C_o or C_{max} (ng/mL)	T_{max} (h)	$AUC_{(o\text{-}inf)}$ (h ng mL^{-1})	Cl (L h^{-1} kg^{-1})	Vdss (L h^{-1} kg^{-1})	$T_{1/2}$ (h)	F (%)
iv	3	1870		600	5.0	1	0.87	
po	10	848	0.25	610			1.4	30
po	100	8960	0.25	11000			2.5	55

[a]After a single intravenous administration of 3 mg/kg dissolved in ethanol/Tween 80/D5% (5/5/90; v/w/v) or after a single oral administration of 10 or 100 mg/kg dissolved in ethanol/Tween 80/glucose 5% (12.5/12.5/75; v/w/v).

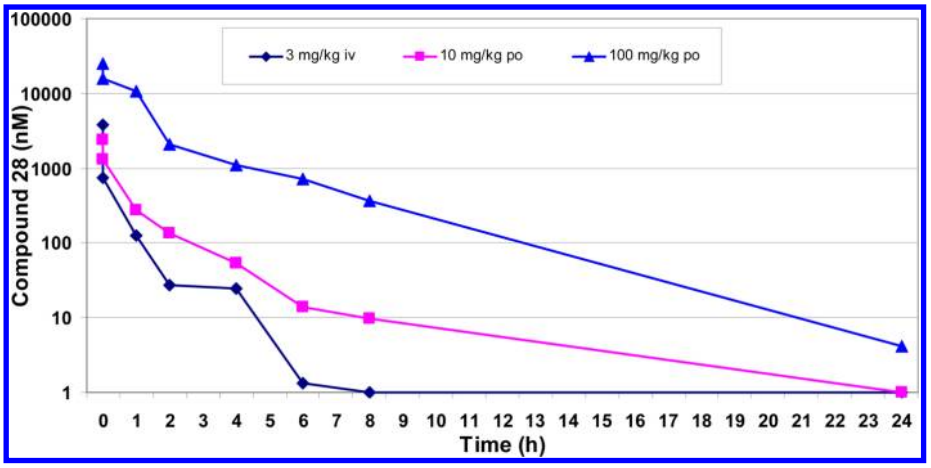

Figure 7. Compound **28** pharmacokinetics at 3 mg/kg iv, 10 mg/kg po, and 100 mg/kg po administrations in mice.

lysine is replaced by a smaller threonine (Thr750) residue in PI3Kδ. The modeled binding of compound **28** in PI3Kδ was corroborated by the observed differences in SAR between PI3Kβ and PI3Kδ described in a previous section for the 4 position of the indoline in this chemical series. The N−H of the amide in the pyrimidone scaffold is pointing toward a partly solvent-exposed region lined with Asp931 and Lys799, supporting the hypothesis that small polar groups would be preferred over a methyl in this position. The (*S*)-methyl on the indoline 2 position of compound **28** is well-defined in the electron density allowing for unambiguous assignment of the absolute stereochemistry for this compound. The observed loss of PI3Kδ but not PI3Kβ potency for compound **28** compared with the (*R*)-isomer (**29**) or the nonmethylated analogue (**6**) is difficult to explain by a simple structural alignment since the only residue within close distance (<6 Å) to the methyl is Met773, which is identical in PI3Kδ (Met752) and adopts a very similar conformation in compound-bound structures from this inhibitor class[19] compared with the one observed in PI3Kβ. One of the main goals of the PI3K crystallography efforts was to understand the structural basis for p110β isoform specificity[35] and to use the information to design more selective PI3Kβ inhibitors. Even if the PI3K structures and associated SAR data reported to date allow for a partial understanding of p110-isoform specificity, important questions related to the underlying mechanisms of lipid kinase isoform selectivity remain largely unexplained. From the structure of compound **28** bound to PI3Kβ, one can observe that the large majority of residues in close contact with the inhibitor are conserved within the four p110 isoforms, and there is no specific interaction that could explain the pronounced affinity of the pyrimidone series and other propeller shaped compounds for p110β and p110δ isoforms compared with p110α or p110γ. A recent mutagenesis study[39] showed that the nature of a residue preceding Met773 in the P-loop has a pivotal role in PI3Kα versus PI3Kβ selectivity. This residue, which is directed away from the ligand binding site, is aromatic in PI3Kβ (Tyr772) and PI3Kδ (Phe751), while in PI3Kα (Ile771) and PI3Kγ (Val803) it is aliphatic. The results of the mutagenesis study support our observations that the underlying mechanisms governing PI3K isoform specificity are complex and not obvious to understand by a straightforward analysis of residue identities and positions in close contact with the bound inhibitors. Structural, biophysical, and in silico analyses are currently being pursued to gain further understanding of the observed PI3K selectivity. The results of these studies will be subject of future publications.

In Vivo Studies. Compound **28** was further evaluated in a pharmacokinetic (PK) study in female Balb/c mice (Table 4). Pharmacokinetic parameters from the intravenous (iv) route indicated a plasma clearance of 5.0 L h^{-1} kg^{-1} comparable to hepatic blood flow in this species (5.2 L h^{-1} kg^{-1}), a Vdss of 1.9 L/kg, and an apparent terminal half-life of $T_{1/2}$ = 0.87 h. Following a single oral administration at 10 mg/kg, mean maximal plasma concentration of compound **28** (848 ng/mL) was rapidly reached between 15 and 30 min postdosing and declined with an apparent terminal half-life value assessed at 1.4 h. The bioavailability of compound **28** was estimated to be over 30%.

With a higher oral dose of 100 mg/kg, plasma exposure was increased more than dose proportionally (19-fold instead of 10) and bioavailability rose to 55%. This over dose proportionality could be explained at least to some extent by the saturation at higher doses of the P-gp efflux pumps leading to an improved absorption. From Figure 7, it was inferred that compound plasma concentration could be maintained above 100 nM for 12 h and above 1 μM for 5 h. The compound was shown to be moderately metabolized by CYPs, the main factor governing compound exposure being the clearance (5.0 L h^{-1} kg^{-1}), which was most likely attributed to phase II metabolism. With these results in hand, it was decided to further evaluate compound **28** in an acute PK/PD experiment in tumor bearing mice at the dose of 100 mg/kg.

The pharmacodynamic (PD) impact of oral administration of compound **28** on a downstream pathway biomarker target in

dx.doi.org/10.1021/jm401642q | J. Med. Chem. 2014, 57, 903−920

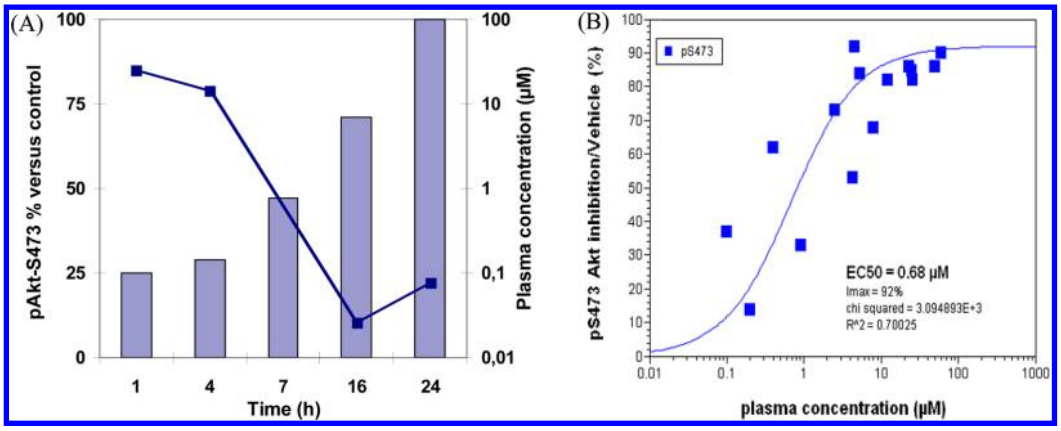

Figure 8. Effect of compound **28** on pAkt-S473 levels. (A) pAkt-S473 modulation in PC3 xenograft model in SCID mice upon treatment with 100 mg/kg po in solution (percentage of pAkt-S473 versus control on the left *Y* axis, and plasma concentration [C] in μM log scale on the right *Y* axis; time in hours on the *X* axis). (B) EC_{50} measured by plotting plasma concentration [C] in μM vs inhibitory effect on pAkt-S473 levels at all time points.

tumor tissue was assessed through an acute PK/PD experiment (Figure 8A). The five time points measurements were performed in PTEN-deficient PC3 prostate tumor xenografts in SCID (severe combined immune deficient) mice, measuring inhibition of Akt phosphorylation at residues S473 and T308 (data not shown). The 100 mg/kg dose used in this experiment was the one selected for the PK/PD screening to evaluate compounds. Oral administration of compound **28** revealed sustained target inhibition (≥50%) of pAkt-S473 for at least 7 h. This biological effect correlated directly with compound exposure in plasma (see Figure 8B and Table 5), and no rate-dependent hysteresis was observed.

Table 5. PK Exposure from Compound 28 PK/PD Study in PC3 Mice Xenograft Model

Dose	100 mg/kg po				
time (h)	1	4	7	16	24
plasma (μM)	24.9	14.2		0.026	0.076

The *in vivo* plasma effective concentration giving 50% PD modulation (EC_{50}) calculated from different experiments was estimated at 0.68 μM (Figure 8B) total drug (0.27 μM free drug), and the EC_{90} was predicted at 6.12 μM total drug (2.5 μM free drug), the protein binding being moderate with a free fraction of approximately 40% in mouse plasma. These results are in agreement with results obtained on tumor cells in which IC_{50} was estimated at 0.05 μM and IC_{90} at 2 μM.

The antitumor effects of compound **28** were then evaluated in PTEN-deficient PC3 prostate tumor subcutaneous xenografts in SCID mice. In this study, tumors were allowed to reach at least 150 mm^3 before treatment, and tumor volume was measured regularly over the treatment period. Mice were treated orally with the compound at the higher dose of 150 mg/kg using a bidaily (BID) schedule in order to favor sustained and potent pathway inhibition, assuming that PI3K pathway shutdown (with concentrations as close as possible to the IC_{90}) should be necessary to reach antitumor effect. Even if the treatment slowed tumor growth, it did not reach statistically significant efficacy as measured by a $\Delta T/\Delta C$ of 61% (p = 0.1925 versus control mice) on treatment day 31 (Figure 9). In this study, treatment with compound **28** induced tumor growth delay at well tolerated doses, with no sign of toxicity and no body weight loss.

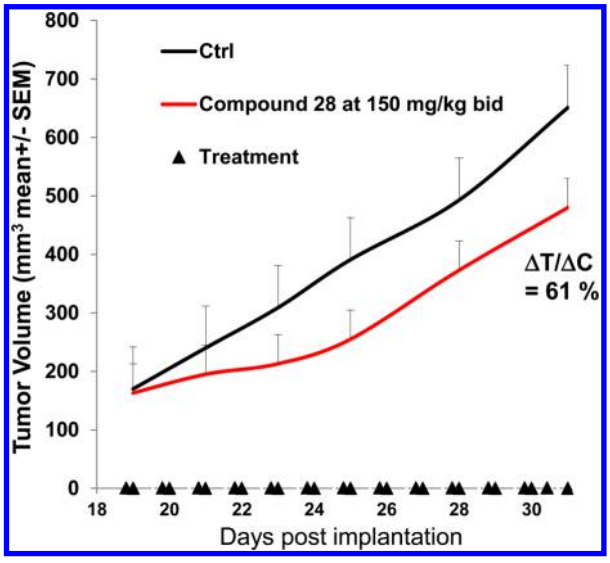

Figure 9. Compound **28** antitumor activity against human PTEN-deficient melanoma PC3-bearing SCID female mice. See Experimental Methods for assay details.

These results recapitulated the published data in which down-regulation of *PIK3CB*, using a shRNA in a PC3 model, led to tumor growth delay but did not to reach statistically significant efficacy as measured by a $\Delta T/\Delta C$ of 49%.[8]

To further investigate on the antitumor potential of compound **28**, its efficacy was examined in other PTEN-deficient tumor indications. Since in melanoma exhibiting PTEN deficiency and $BRAF^{V600E}$ mutation, PTEN deficiency has been reported to play a role in the resistance to BRAF inhibitors,[40] the compound was evaluated in UACC-62 melanoma model exhibiting concomitant $BRAF^{V600E}$ mutation and PTEN loss. Compound **28** was evaluated first in an acute PK/PD experiment in UACC-62 tumor-bearing mice at the dose of 200 mg/kg, in order to examine whether a higher dose would allow it to shutdown the PI3Kβ pathway for a longer time period. Oral administration of compound **28** revealed sustained target inhibition (>50%) of pAkt-S473 for at least 6 h (concentration at this time was 4.55 μM total drug and 1.82 μM free drug.), but no pathway inhibition was observed at 16 h. This biological effect correlated directly with compound exposure in plasma (Figure 10). In the

dx.doi.org/10.1021/jm401642q | J. Med. Chem. 2014, 57, 903−920

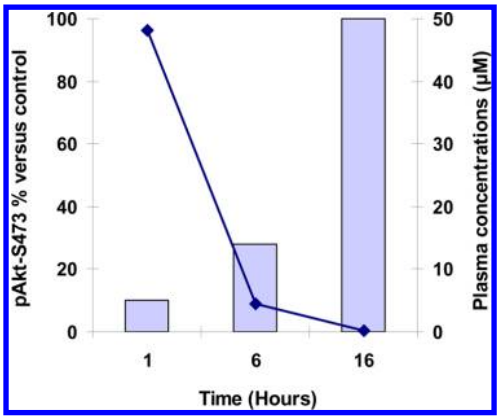

Figure 10. Effect of compound **28** at 200 mg/kg po on pAKT-S473 expression in tumors from UACC-62 tumor-bearing SCID mice and plasma exposure after treatment. See Experimental Methods for assay details.

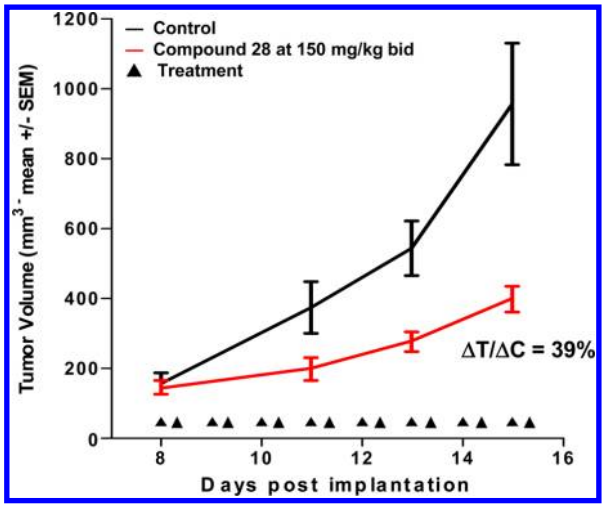

Figure 11. Compound **28** antitumor activity against human $BRAF^{V600E}$/PTEN-deficient melanoma UACC-62-bearing SCID female mice. See Experimental Methods for assay details.

UACC-62 tumor cell line assay, compound **28** inhibited pAkt-S473 with a measured IC_{50} at 0.06 μM and an estimated IC_{90} at 2 μM.

The compound was then evaluated for its antitumor effects in UACC-62 melanoma subcutaneous xenografts in SCID mice. In this study, tumors were allowed to reach at least 150 mm^3 before treatment, and tumor volume was measured regularly over the treatment period. Mice were treated orally with the compound at the dose of 150 mg/kg using a bidaily (BID) schedule in order to favor sustained pathway inhibition and allow comparison with the study performed in PC3 model. Compound **28** treatment led to a statistically significant tumor growth inhibition as measured by a $\Delta T/\Delta C$ of 39% (p = 0.054 versus control mice) on day 15 post-tumor implantation (Figure 11). In this study, compound **28** was well tolerated at the active dose, with no sign of toxicity and no body weight loss.

The results obtained from UACC-62 melanoma and PC3 prostate efficacy studies show that PTEN deficiency appears as necessary but not sufficient for sensitivity to PI3Kβ pathway inhibition. Other genetic events (different genetic background between both models) and the tumor indication may impact model sensitivity and addiction to PI3Kβ pathway. This is not unusual and has already been observed for targeted therapy: for example, the modest clinical activity of BRAF inhibitor vemurafenib in $BRAF^{V600E}$ metastatic colorectal cancers compared with that observed in $BRAF^{V600E}$ melanoma patients suggests important differences in the biology of BRAF mutant tumors in different cancer types.[41,42]

Compound **28** was then evaluated in a preliminary pharmacokinetic (PK) study in female nude rats showing a bioavailability of 70% (Table 6).

Finally compound **28** was evaluated in a pharmacokinetic (PK) study in male Beagle dogs showing a bioavailability of 67% (Table 7). The improved pharmacokinetic profile obtained in dogs (especially AUC) could be due, to some extent, to the higher stability in microsomes obtained in this species (lability in dog liver microsome was 5%)

Compound **28** has been found to display antitumor efficacy in human PTEN-deficient melanoma models in mice as a single agent. Combination studies[43] have been shown to bring a therapeutic benefit, and the detailed experimental results will be the subject of a forthcoming paper.

Following these encouraging preliminary *in vivo* results and pharmacokinetic properties compound **28** was further evaluated in preclinical studies involving process development large scale synthesis and preliminary toxicity studies.

CHEMISTRY

The intermediates **1**, **2**, **3**, and **4** have been described previously.[17−19] Compound **1** was efficiently obtained by a one-pot reaction between morpholine and an excess of commercially available ethyl 3-amino-3-ethoxyacrylate hydrochloride in the presence of *N*,*N*-diisopropylethylamine (DIPEA) in ethanol under reflux, as previously reported.[17] Compound **1** was converted into **3** via methylation using methyl iodide in dioxane in the presence of cesium carbonate at 40 °C under argon. The two sodium salts **2** and **4** were obtained at room temperature by saponification of the esters **1** and **3**, respectively, in tetrahydrofuran with sodium hydroxide. The final compounds where then obtained via condensation with the appropriate indoline as depicted in Scheme 1.

Certain indolines were not commercially available and were prepared by reduction of the corresponding indoles, using sodium cyanoborohydride in trifluoroacetic acid as described in Scheme 2.

Table 6. Pharmacokinetic Plasma Parameters of Compound 28 in Female Nude Rats[a]

route	dose (mg/kg)	C_o or C_{max} (ng/mL)	T_{max} (h)	$AUC_{(o\text{-}inf)}$ (h ng mL^{-1})	Cl (L h^{-1} kg^{-1})	Vdss (L h^{-1} kg^{-1})	$T_{1/2}$ (h)	F(%)
iv	3	1200		864	3.4	8.1	0.87	
po	10	1460	0.25	2410			6.9	70

[a]After a single intravenous administration of 3 mg/kg in solution in 2.5% ethanol, 7.5% PS80 in glucose 5% and oral administration of 10 mg/kg in solution in 12.5% ethanol, 12.5% PS80 in glucose 5%, pH 3.

dx.doi.org/10.1021/jm401642q | J. Med. Chem. 2014, 57, 903−920

Table 7. Pharmacokinetic Plasma Parameters of Compound 28 in Male Beagle Dogs[a]

route	dose (mg/kg)	C_o or C_{max} (ng/mL)	T_{max} (h)	$AUC_{(o\text{-}inf)}$ (h ng mL^{-1})	Cl (L h^{-1} kg^{-1})	Vdss (L h^{-1} kg^{-1})	$T_{1/2}$ (h)	F(%)
iv	3	4920	0.5	6580	0.4	>3	>5	
po	10	4770	0.5	14 000			4.5	67

[a]After a single intravenous administration of 3 mg/kg in solution in EtOH/solutol/G5 (2.5/7.5/90) and oral administration of 10 mg/kg in solution in EtOH/solutol/G5 (2.5/7.5/90).

Scheme 1. Synthesis of Compounds 7−29 and Intermediates 1−4[a]

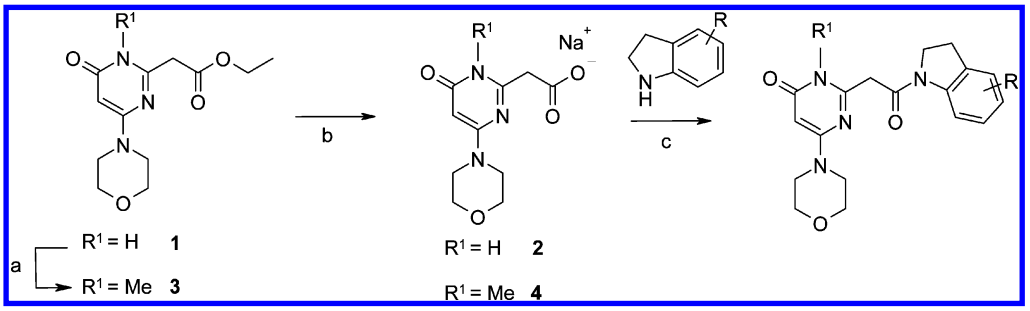

[a]Reagents and conditions: (a) MeI, Cs_2CO_3, dioxane under argon, 40 °C, 16 h, 75%; (b) NaOH, THF, rt, 48 h, 100%; (c) EDCI, pyridine, DMF, rt, 16 h, 6−78%.

Scheme 2. Synthesis of Some Intermediate Indolines from the Indoles, 30−31[a]

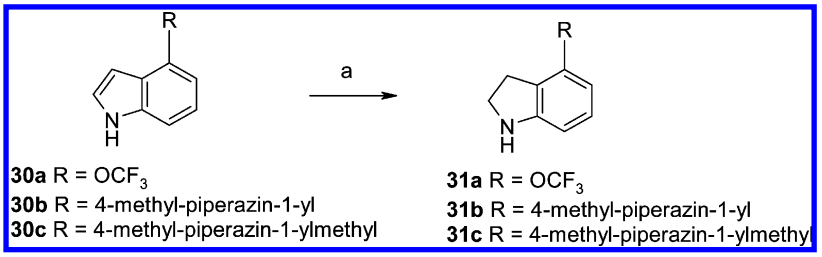

[a]Reagents and conditions: (a) $NaBH_3CN$, TFA, 0 °C, 34 h, 20−75%; or $NaBH_3CN$, AcOH, RT, 2 h, 76−80%; see Experimental Methods for details.

CONCLUSION

A new series of high LE pyrimidone indoline amide PI3Kβ inhibitors prepared by a new short and efficient synthesis, utilizing the newly discovered intermediate compound **1**, has been identified.[19] Series progression, through SAR analysis, physicochemical optimization, and *in vitro* pharmacokinetic optimization has led to the discovery of potent compounds, but lacking intrinsic aqueous solubility. Further analysis of compound **7** and especially X-ray crystal determination has revealed a strong network of hydrogen bond and hydrophobic interactions. Disruption of compound **7** crystal packing by careful introduction of a methyl group at suitable positions has led to the isolation of the soluble compound **24**. Chiral separation allowed the characterization of both (*R*)- and (*S*)-enantiomers, highlighting two different selectivity profiles. The (*S*)-enantiomer, compound **28**, was selected as a potent and soluble PI3Kβ inhibitor, selective versus other protein and lipid kinases. Compound **28** was also crystallized in PI3Kβ where it binds to the ATP pocket in an analogous conformation to what has previously been reported for similar PI3Kβ inhibitors in PI3Kγ and PI3Kδ.[16,17] Although the binding mode observed in these structures sheds light on important features in the SAR for the pyrimidone series, the origins of PI3Kβ isoform specificity remain elusive. X-ray crystal structures and biophysical and in silico modeling analyses are currently being investigated to gain further understanding of the observed PI3K selectivity. Compound **28** displayed PK properties in mice warranting additional evaluation *in vivo*. It was shown to efficiently inhibit pAkt-S473 in PTEN-deficient PC3 and UACC-62 tumor models for at least 6 h at the doses of 100 and 200 mg/kg, respectively. Pathway modulation translated to antitumor efficacy with significant activity in particular in $BRAF^{V600E}$ mutant/PTEN-deficient UACC-62 melanoma model. Complementary evaluation and especially pharmacokinetic experiments in dogs have shown that compound **28** was orally absorbed and deserved further preclinical investigation. In vivo pharmacology studies of compound **28** as a single agent and in combination in PTEN-deficient xenograft mice models[43] have been recently presented[44,45] and will be the subject of future publications. Compound **28** (SAR260301) was submitted to preclinical studies and, following favorable toxicity profile and comfortable therapeutic index, entered clinical trials phase I/Ib in 2012.

EXPERIMENTAL METHODS

Chemistry. The nomenclature of the compounds was carried out with the ACDLABS software, version 11.01. All solvents and reagents obtained from commercial sources were used without further purification. Thin layer chromatography was carried out on Merck silica gel 60 F254 glass plates. Flash chromatography was performed using prepacked Merck silica gel cartridges (15−40 μm). The microwave oven used was a Biotage, InitiatorTM 2.0, 400 W max, 2450 MHz instrument. The ^{1}H NMR spectra at 400 MHz and the ^{1}H NMR spectra at 500 MHz were performed on a Bruker Avance DRX-400 or Bruker Avance DPX-500 spectrometer with the chemical shifts (δ in ppm) in the solvent dimethyl sulfoxide-d_6 (d_6-DMSO) referenced

dx.doi.org/10.1021/jm401642q | J. Med. Chem. 2014, 57, 903−920

at 2.5 ppm at a temperature of 303 K, and coupling constants (*J*) are given in hertz.

The mass spectra (MS) were obtained by methods A and B.

Method A: Waters UPLC-SQD instrument; ionization, positive or negative mode electrospray (ES+ and ES−) or both; chromatographic conditions, column Acquity BEH C_{18} 1.7 μM, 2.1 mm × 50 mm; solvents (A) H_2O (0.1% formic acid), (B) CH_3CN (0.1% formic acid); column temperature 50 °C; flow rate 1 mL/min; gradient (2 min) from 5% to 50% of B in 0.8 min; 1.2 min 100% of B; 1.85 min 100% of B; 1.95 min 5% of B; retention time = T_r (min).

Method B: Waters ZQ instrument; ionization, positive or negative mode electrospray (ES+ or ES−) or both; chromatographic conditions, column XBridge C_{18} 2.5 μM, 3 mm × 50 mm; solvents (A) H_2O (0.1% formic acid), (B) CH_3CN (0.1% formic acid); column temperature 70 °C; flow rate 0.9 mL/min; gradient (7 min) from 5% to 100%.

Purities for final compounds were measured using UV detection at 220 nm and are ≥95.0%.

*2-[2-(2,3-Dihydro-1H-indol-1-yl)-2-oxoethyl]-6-(morpholin-4-yl)-pyrimidin-4(3H)-one (**7**).* To a solution of **2**[18] (261 mg, 1 mmol) in 4 mL of dimethylformamide were introduced pyridine (0.16 mL, 2 mmol), *N*-[3-(dimethylamino)propyl]-*N*′-ethylcarbodiimide hydrochloride (EDCI; 0.25 g, 1.3 mmol), and 2,3-dihydro-1*H*-indole (238 mg, 2 mmol). The reaction mixture was stirred at ambient temperature for 16 h and then evaporated to dryness under reduced pressure. Water and ethyl acetate were added, and the resulting mixture was stirred for 30 min. The precipitate formed was filtered off, washed with water, diethyl ether, and petroleum ether, and dried to give **7** (230 mg, 68%) as a pale pink solid, mp >260 °C. ^{1}H NMR (400 MHz): 3.17 (t, *J* = 8.3 Hz, 2H); 3.41 (m, 4H); 3.60 (m, 4H); 3.75 (s, 2H); 4.14 (t, *J* = 8.3 Hz, 2H); 5.21 (s, 1H); 7.01 (t, *J* = 7.6 Hz, 1H); 7.16 (t, *J* = 7.6 Hz, 1H); 7.25 (d, *J* = 7.6 Hz, 1H); 8.02 (d, *J* = 7.6 Hz, 1H); 11.61 (broad s, 1H). Mass spectrometry: method A; T_r (min) = 0.64. $[M + H]^+$ *m*/*z* 341. $[M - H]^-$ *m*/*z* 339.

*2-[2-(5-Fluoro-2,3-dihydroindol-1-yl)-2-oxoethyl]-6-morpholin-4-yl-3H-pyrimidin-4-one (**8**).* By a similar procedure to that described for the synthesis of **6** using **2** (261 mg, 1 mmol) and 5-fluoro-2,3-dihydro-1*H*-indole (274 mg, 2 mmol), **8** (197 mg, 55%) was obtained as a pale pink powder, mp 264 °C. ^{1}H NMR (400 MHz): 3.18 (t, *J* = 8.2 Hz, 2H); 3.42 (m, 4H); 3.60 (m, 4H); 3.74 (s, 2H); 4.16 (t, *J* = 8.2 Hz, 2H); 5.20 (s, 1H); 6.98 (broad t, *J* = 8.9 Hz, 1H); 7.12 (broad d, *J* = 8.9 Hz, 1H); 8.00 (dd, *J* = 5.3 and 8.9 Hz, 1H); 11.61 (broad m, 1H). Mass spectrometry: method A; T_r (min) = 0.70; $[M + H]^+$ *m*/*z* 359; $[M - H]^-$ *m*/*z* 357.

*2-[2-(5-Chloro-2,3-dihydroindol-1-yl)-2-oxoethyl]-6-morpholin-4-yl-3H-pyrimidin-4-one (**9**).* By a similar procedure to that described for the synthesis of **6** using **2** (261 mg, 1 mmol) and 5-chloro-2,3-dihydro-1*H*-indole (307 mg, 2 mmol), **9** (255 mg, 71%) was obtained as a white powder, mp >260 °C. ^{1}H NMR (400 MHz): 3.18 (t, *J* = 8.3 Hz, 2H); 3.41 (m, 4H); 3.60 (m, 4H); 3.75 (s, 2H); 4.16 (t, *J* = 8.3 Hz, 2H); 5.20 (s, 1H); 7.21 (broad d, *J* = 8.6 Hz, 1H); 7.32 (broad s, 1H); 7.99 (d, *J* = 8.6 Hz, 1H); 11.61 (broad m, 1H). Mass spectrometry: method B; T_r (min) = 3.42; $[M - H]^-$ *m*/*z* 373.

*2-[2-(4-Fluoro-2,3-dihydro-1H-indol-1-yl)-2-oxoethyl]-6-(morpholin-4-yl)pyrimidin-4(3H)-one (**10**).* By a similar procedure to that described for the synthesis of **6** using **2** (261 mg, 1 mmol) and 4-fluoro-2,3-dihydro-1*H*-indole (274 mg, 2 mmol), **10** (250 mg, 70%) was obtained as a white solid, mp >260 °C. ^{1}H NMR (400 MHz): 3.20 (t, *J* = 8.4 Hz, 2H); 3.41 (m, 4H); 3.61 (m, 4H); 3.76 (s, 2H); 4.21 (t, *J* = 8.4 Hz, 2H); 5.21 (s, 1H); 6.86 (t, *J* = 8.6 Hz, 1H); 7.12 to 7.31 (m, 1H); 7.84 (d, *J* = 8.1 Hz, 1H); 11.61 (broad s, 1H). Mass spectrometry: method B; T_r (min) = 3.20; $[M + H]^+$ *m*/*z* 359; $[M - H]^-$ *m*/*z* 357.

*2-[2-(4-Chloro-2,3-dihydro-1H-indol-1-yl)-2-oxoethyl]-6-(morpholin-4-yl)pyrimidin-4(3H)-one (**11**).* By a similar procedure to that described for the synthesis of **6** using **2** (261 mg, 1 mmol) and 4-chloro-2,3-dihydro-1*H*-indole (307 mg, 2 mmol), **11** (247 mg, 66%) was obtained as a white solid, mp >260 °C. ^{1}H NMR (400 MHz): 3.18 (t, *J* = 8.4 Hz, 2H); 3.41 (m, 4H); 3.60 (m, 4H); 3.76 (s, 2H); 4.20 (t, *J* = 8.4 Hz, 2H); 5.21 (s, 1H); 7.09 (d, *J* = 8.1 Hz, 1H); 7.22 (t, *J* = 8.1 Hz, 1H); 7.97 (d, *J* = 8.1 Hz, 1H); 11.62 (broad s, 1H). Mass spectrometry: method B; T_r (min) = 3.46; $[M + H]^+$ *m*/*z* 375; $[M - H]^-$ *m*/*z* 373.

*2-[2-(4-Bromo-2,3-dihydroindol-1-yl)-2-oxoethyl]-6-morpholin-4-yl-3H-pyrimidin-4-one (**12**).* By a similar procedure to that described for the synthesis of **6** using **2** (261 mg, 1 mmol) and 4-bromo-2,3-dihydro-1*H*-indole (402 mg, 2 mMol), **12** (303 mg, 72%) was obtained as a white powder, mp 219 °C. ^{1}H NMR (400 MHz): 3.14 (t, *J* = 8.4 Hz, 2H); 3.41 (m, 4H); 3.61 (m, 4H); 3.76 (s, 2H); 4.19 (t, *J* = 8.4 Hz, 2H); 5.21 (s, 1H); 7.14 (t, *J* = 8.1 Hz, 1H); 7.23 (broad d, *J* = 8.1 Hz, 1H); 8.01 (broad d, *J* = 8.1 Hz, 1H); 11.62 (broad m, 1H). Mass spectrometry: method A; T_r (min) = 0.88; $[M + H]^+$ *m*/*z* 419; $[M - H]^-$ *m*/*z* 417.

*2-[2-(4-Methyl-2,3-dihydro-1H-indol-1-yl)-2-oxoethyl]-6-(morpholin-4-yl)pyrimidin-4(3H)-one (**13**).* By a similar procedure to that described for the synthesis of **6** using **2** (261 mg, 1 mmol) and 4-methyl-2,3-dihydro-1*H*-indole hydrochloride (339 mg, 2 mmol), **13** (22 mg, 6%) was obtained as a fuchsia crystalline powder, mp >260 °C. ^{1}H NMR (400 MHz): 2.21 (s, 3H); 3.08 (t, *J* = 8.3 Hz, 2H); 3.42 (m, 4H); 3.61 (m, 4H); 3.75 (s, 2H); 4.15 (t, *J* = 8.3 Hz, 2H); 5.20 (s, 1H); 6.85 (d, *J* = 8.0 Hz, 1H); 7.07 (t, *J* = 8.0 Hz, 1H); 7.85 (d, *J* = 8.0 Hz, 1H); 11.62 (broad m, 1H). Mass spectrometry: method B; T_r (min) = 3.31; $[M + H]^+$ *m*/*z* 355; $[M - H]^-$ *m*/*z* 353.

*2-[2-(4-Methoxy-2,3-dihydroindol-1-yl)-2-oxoethyl]-6-morpholin-4-yl-3H-pyrimidin-4-one (**14**).* By a similar procedure to that described for the synthesis of **6** using **2** (261 mg, 1 mmol) and 4-methoxy-2,3-dihydro-1*H*-indole (308 mg, 2 mMol), **14** (269 mg, 73%) was obtained as a pink powder, mp >260 °C. ^{1}H NMR (400 MHz): 3.04 (t, *J* = 8.2 Hz, 2H); 3.41 (m, 4H); 3.61 (m, 4H); 3.74 (s, 2H); 3.79 (s, 3H); 4.14 (t, *J* = 8.2 Hz, 2H); 5.20 (s, 1H); 6.70 (broad d, *J* = 7.9 Hz, 1H); 7.15 (t, *J* = 7.9 Hz, 1H); 7.64 (broad d, *J* = 7.9 Hz, 1H); 11.61 (broad m, 1H). Mass spectrometry: method A; T_r (min) = 0.75; $[M + H]^+$ *m*/*z* 371; $[M - H]^-$ *m*/*z* 369.

*6-(Morpholin-4-yl)-2-{2-oxo-2-[4-(trifluoromethyl)-2,3-dihydro-1H-indol-1-yl]ethyl}pyrimidin-4(3H)-one (**15**).* By a similar procedure to that described for the synthesis of **6** using **2** (977 mg, 3.74 mmol) and 4-trifluoromethyl-2,3-dihydro-1*H*-indole (700 mg, 5.1 mmol), followed by a purification on silica gel (DCM/MeOH, 95/5), **15** (220 mg, 14%) was obtained as a white powder. ^{1}H NMR (400 MHz): 3.27 to 3.45 (m partially masked, 6H); 3.60 (m, 4H); 3.79 (s, 2H); 4.22 (t, *J* = 8.6 Hz, 2H); 5.22 (s, 1H); 7.34 (d, *J* = 8.1 Hz, 1H); 7.41 (t, *J* = 8.1 Hz, 1H); 8.30 (d, *J* = 8.1 Hz, 1H); 11.64 (broad m, 1H). Mass spectrometry: method A; T_r (min) = 0.82; $[M + H]^+$ *m*/*z* 409; $[M - H]^-$ *m*/*z* 407.

*6-(Morpholin-4-yl)-2-{2-oxo-2-[4-(trifluoromethoxy)-2,3-dihydro-1H-indol-1 yl]ethyl}pyrimidin-4(3H)-one (**16**).* By a similar procedure to that described for the synthesis of **6** using **2** (110 mg, 0.42 mmol) and 4-(trifluoromethoxy)-2,3-dihydro-1*H*-indole **31a** (178 mg, 1.14 mmol), **16** (97 mg, 54%) was obtained as a white powder, mp >260 °C. ^{1}H NMR (400 MHz): 3.21 (t, *J* = 8.6 Hz, 2H); 3.41 (m, 4H); 3.60 (m, 4H); 3.77 (s, 2H); 4.22 (t, *J* = 8.6 Hz, 2H); 5.21 (s, 1H); 7.02 (d, *J* = 8.1 Hz, 1H); 7.32 (t, *J* = 8.1 Hz, 1H); 8.02 (d, *J* = 8.1 Hz, 1H); 11.62 (broad s, 1H). Mass spectrometry: method A; T_r (min) = 0.85; $[M + H]^+$ *m*/*z* 425; $[M - H]^-$ *m*/*z* 423.

*6-(Morpholin-4-yl)-2-[2-oxo-2-(4-phenyl-2,3-dihydro-1H-indol-1-yl)-ethyl]pyrimidin-4(3H)-one (**17**).* By a similar procedure to that described for the synthesis of **6** using **2** (250 mg, 0.95 mmol) and 4-phenyl-2,3-dihydro-1*H*-indole (210 mg, 1.08 mmol), followed by purification on silica gel (DCM/MeOH, 90/10), **17** (232 mg, 58%) was obtained as a pink powder, mp 266 °C. ^{1}H NMR (400 MHz): 3.22 (t, *J* = 8.7 Hz, 2H); 3.42 (m, 4H); 3.61 (m, 4H); 3.78 (s, 2H); 4.14 (t, *J* = 8.7 Hz, 2H); 5.21 (s, 1H); 7.07 (d, *J* = 7.8 Hz, 1H); 7.28 (t, *J* = 7.8 Hz, 1H); 7.36 to 7.51 (m, 5H); 8.08 (d, *J* = 7.8 Hz, 1H); 11.62 (broad s, 1H). Mass spectrometry: method A; T_r (min) = 0.89; $[M + H]^+$ *m*/*z* 417; $[M - H]^-$ *m*/*z* 415.

*6-(Morpholin-4-yl)-2-{2-oxo-2-[4-(pyridin-2-yl)-2,3-dihydro-1H-indol-1-yl]ethyl}pyrimidin-4(3H)-one (**18**).* By a similar procedure to that described for the synthesis of **6** using **2** (27 mg, 0.1 mmol) and 4-pyridin-2-yl-2,3-dihydro-1*H*-indole (25 mg, 0.13 mmol), **18** (27 mg, 62%) was obtained as a purple solid. ^{1}H NMR (400 MHz): 3.37 to 3.46 (m, *J* = 5.9 Hz, 6H); 3.61 (m, 4H); 3.79 (broad s, 2H); 4.16

dx.doi.org/10.1021/jm401642q | J. Med. Chem. 2014, 57, 903−920

(t, J = 8.6 Hz, 2H); 5.23 (s, 1H); 7.26 to 7.47 (m, 3H); 7.77 (d, J = 8.3 Hz, 1H); 7.93 (t, J = 8.1 Hz, 1H); 8.16 (d, J = 8.1 Hz, 1H); 8.69 (d, J = 5.6 Hz, 1H); 11.69 (s large, 1H). Mass spectrometry: method A; T_r (min) = 0.53; $[M + H]^+$ m/z 418; $[M - H]^-$ m/z 416.

*6-(Morpholin-4-yl)-2-{2-oxo-2-[4-(pyridin-3-yl)-2,3-dihydro-1H-indol-1-yl]ethyl}pyrimidin-4(3H)-one (**19**).* By a similar procedure to that described for the synthesis of **6** using **2** (27 mg, 0.1 mmol) and 4-pyridin-3-yl-2,3-dihydro-1*H*-indole (25 mg, 0.13 mmol), **19** (31 mg, 78%) was obtained as a pink solid. ^{1}H NMR (400 MHz): 3.25 (t, J = 8.1 Hz, 2H); 3.43 (m, 4H); 3.61 (m, 4H); 3.79 (s, 2H); 4.16 (t, J = 8.4 Hz, 2H); 5.22 (s, 1H); 7.14 (d, J = 7.8 Hz, 1H); 7.33 (t, J = 7.9 Hz, 1H); 7.57 (dd, J = 4.9 and 7.8 Hz, 1H); 8.02 (d, J = 8.1 Hz, 1H); 8.13 (d, J = 8.1 Hz, 1H); 8.63 (dd, J = 1.7 and 4.9 Hz, 1H); 8.76 (dd, J = 0.6 and 1.8 Hz, 1H); 11.65 (broad s, 1H). Mass spectrometry: method A; T_r (min) = 0.45; $[M + H]^+$ m/z 418; $[M - H]^-$ m/z 416.

*6-(Morpholin-4-yl)-2-{2-oxo-2-[4-(pyridin-4-yl)-2,3-dihydro-1H-indol-1-yl]ethyl}pyrimidin-4(3H)-one (**20**).* By a similar procedure to that described for the synthesis of **6** using **2** (27 mg, 0.1 mmol) and 4-pyridin-4-yl-2,3-dihydro-1*H*-indole (25 mg, 0.13), **20** (28 mg, 70%) was obtained as a pink solid. ^{1}H NMR (400 MHz): 3.27 (masked m, 2H); 3.41 (m, 4H); 3.61 (m, 4H); 3.79 (s, 2H); 4.16 (t, J = 8.4 Hz, 2H); 5.22 (s, 1H); 7.18 (d, J = 7.6 Hz, 1H); 7.35 (t, J = 7.9 Hz, 1H); 7.61 (d, J = 6.4 Hz, 2H); 8.16 (d, J = 8.3 Hz, 1H); 8.69 (d, J = 6.1 Hz, 2H); 11.66 (broad s, 1H). Mass spectrometry: method A; T_r (min) = 0.40; $[M + H]^+$ m/z 418; $[M - H]^-$ m/z 416.

*2-{2-[4-(4-Methylpiperazin-1-yl)-2,3-dihydro-1H-indol-1-yl]-2-oxoethyl}-6-(morpholin-4-yl)pyrimidin-4(3H)-one (**21**).* By a similar procedure to that described for the synthesis of **6** using **2** (288 mg, 1.1 mmol) and 4-(4-methyl-piperazin-1-yl)-2,3-dihydro-1*H*-indole **31b** (160 mg, 0.73 mmol), followed by purification on silica gel (DCM/NH_3 7 N in MeOH, 90/10), **21** (29 mg, 6%) was obtained as a white powder. ^{1}H NMR (400 MHz): 2.23 (s, 3H); 2.44 (masked m, 4H); 2.93 (m, 4H); 3.06 (t, J = 8.3 Hz, 2H); 3.43 (m, 4H); 3.60 (m, 4H); 3.74 (s, 2H); 4.11 (t, J = 8.2 Hz, 2H); 5.20 (s, 1H); 6.67 (d, J = 7.6 Hz, 1H); 7.11 (t, J = 8.4 Hz, 1H); 7.71 (d, J = 8.1 Hz, 1H); 11.60 (s, 1H). Mass spectrometry: method A; T_r (min) = 0.36; $[M + H]^+$ m/z 439; $[M - H]^-$ m/z 437.

*2-(2-{4-[(4-Methylpiperazin-1-yl)methyl]-2,3-dihydro-1H-indol-1-yl}-2-oxoethyl)-6-(morpholin-4-yl)pyrimidin-4(3H)-one (**22**).* By a similar procedure to that described for the synthesis of **6** using **2** (410 mg, 1.57 mmol) and 4-(4-methyl-piperazin-1-ylmethyl)-2,3-dihydro-1*H*-indole **31c** (400 mg, 1.73 mmol), followed by purification on silica gel (DCM/NH_3 7 N in MeOH, 90/10), **22** (120 mg, 17%) was obtained as a white powder. ^{1}H NMR (300 MHz): 2.14 (s, 3H); 2.24 to 2.41 (m, 8H); 3.17 (t, J = 8.4 Hz, 2H); 3.38 to 3.47 (m, 6H); 3.60 (m, 4H); 3.75 (s, 2H); 4.15 (t, J = 8.1 Hz, 2H); 5.21 (s, 1H); 6.95 (d, J = 7.6 Hz, 1H); 7.12 (t, J = 7.8 Hz, 1H); 7.93 (d, J = 7.8 Hz, 1H); 11.61 (broad s, 1H). Mass spectrometry: method A; T_r (min) = 0.36; $[M + H]^+$ m/z 453; $[M - H]^-$ m/z 451.

*2-[2-(2,3-Dihydro-1H-indol-1-yl)-2-oxoethyl]-3-methyl-6-(morpholin-4-yl)pyrimidin-4(3H)-one (**23**).* By a similar procedure to that described for the synthesis of **6** using **4**[18] (200 mg, 1.24 mmol) and 2,3-dihydro-1*H*-indole (174 mg, 1.29 mmol), followed by a purification on silica gel (DCM/MeOH, 93/7), **23** (52 mg, 20%) was obtained as a white powder, mp >250 °C. ^{1}H NMR (400 MHz): 3.17 (t, J = 8.4 Hz, 2H); 3.32 (s, 3H); 3.39 (m, 4H); 3.58 (m, 4H); 4.11 (s, 2H); 4.17 (t, J = 8.4 Hz, 2H); 5.36 (s, 1H); 7.02 (t, J = 7.5 Hz, 1H); 7.16 (t, J = 7.5 Hz, 1H); 7.26 (d, J = 7.5 Hz, 1H); 8.01 (d, J = 7.5 Hz, 1H). Mass spectrometry: method A; T_r (min) = 0.68; $[M + H]^+$ m/z 355; $[M - H]^-$ m/z 353.

*2-[2-(2-Methyl-2,3-dihydro-1H-indol-1-yl)-2-oxoethyl]-6-(morpholin-4-yl)pyrimidin-4(3H)-one (**24**).* By a similar procedure to that described for the synthesis of **6** using **2** (500 mg, 1.92 mmol) and 2-methyl-2,3-dihydro-1*H*-indole (510 mg, 3.40 mmol), **24** (400 mg, 59%) was obtained as a white powder, mp 172 °C. ^{1}H NMR (400 MHz): 1.26 (d, J = 6.1 Hz, 3H); 2.65 to 2.72 (m, 1H); 3.18 to 3.44 (m partially masked, 5H); 3.54 to 3.63 (m, 4H); 3.72 (d, J = 15.7 Hz, 1H); 3.92 (d, J = 15.7 Hz, 1H); 4.71 (m, 1H); 5.20 (s, 1H); 7.04 (t, J = 7.8 Hz, 1H); 7.18 (t, J = 7.8 Hz, 1H); 7.29 (d, J = 7.8 Hz, 1H); 7.96 (d, J = 7.8 Hz, 1H); 11.69 (broad m, 1H). Mass spectrometry: method A; T_r (min) = 0.70; $[M + H]^+$ m/z 355; $[M - H]^-$ m/z 353.

*2-[2-(2,2-Dimethyl-2,3-dihydro-1H-indol-1-yl)-2-oxoethyl]-6-(morpholin-4-yl)pyrimidin-4(3H)-one (**25**).* By a similar procedure to that described for the synthesis of **6** using **2** (210 mg, 1.30 mmol) and 2,2-dimethyl-2,3-dihydro-1*H*-indole (130 mg, 1.25 mmol), **25** (75 mg, 25%) was obtained as a white powder, mp 237 °C. ^{1}H NMR (400 MHz): 1.54 (s, 6H); 3.00 (s, 2H); 3.40 (m, 4H); 3.59 (m, 4H); 3.88 (s, 2H); 5.20 (s, 1H); 7.02 (t, J = 7.1 Hz, 1H); 7.16 (t, J = 7.1 Hz, 1H); 7.24 (d, J = 7.1 Hz, 1H); 7.47 (broad s, 1H); 11.64 (broad s, 1H). Mass spectrometry: method A; T_r (min) = 0.77; $[M + H]^+$ m/z 369; $[M - H]^-$ m/z 367.

*2-[2-(3-Methyl-2,3-dihydro-1H-indol-1-yl)-2-oxoethyl]-6-(morpholin-4-yl)pyrimidin-4(3H)-one (**26**).* By a similar procedure to that described for the synthesis of **6** using **2** (500 mg, 1.92 mmol) and 3-methylindoline (170 mg, 1.14 mmol), **26** (367 mg, 54%) was obtained as a white crystalline powder, mp >260 °C. ^{1}H NMR (400 MHz): 1.29 (d, J = 6.8 Hz, 3H); 3.42 (m, 4H); 3.49 (m, 1H); 3.60 (m, 4H); 3.68 (dd, J = 6.8 and 9.8 Hz, 1H); 3.75 (s, 2H); 4.33 (t, J = 9.8 Hz, 1H); 5.21 (s, 1H); 7.04 (t, J = 7.8 Hz, 1H); 7.18 (t, J = 7.8 Hz, 1H); 7.27 (d, J = 7.8 Hz, 1H); 8.01 (d, J = 7.8 Hz, 1H); 11.62 (broad m, 1H). Mass spectrometry: method A; T_r (min) = 0.73; $[M + H]^+$ m/z 355; $[M - H]^-$ m/z 353.

*2-[2-(3,3-Dimethyl-2,3-dihydro-1H-indol-1-yl)-2-oxoethyl]-6-(morpholin-4-yl)pyrimidin-4(3H)-one (**27**).* By a similar procedure to that described for the synthesis of **6** using **2** (177 mg, 0.68 mmol) and 3,3-methylindoline (236 mg, 1.45 mmol), **27** (134 mg, 54%) was obtained as a pink solid, mp 248 °C. ^{1}H NMR (400 MHz): 1.31 (s, 6H); 3.42 (m, 4H); 3.59 (m, 4H); 3.75 (s, 2H); 3.91 (s, 2H); 5.20 (s, 1H); 7.05 (t, J = 7.6 Hz, 1H); 7.18 (t, J = 7.6 Hz, 1H); 7.27 (d, J = 7.6 Hz, 1H); 8.00 (d, J = 7.6 Hz, 1H); 11.61 (broad m, 1H). Mass spectrometry: method A; T_r (min) = 0.77; $[M + H]^+$ m/z 369; $[M - H]^-$ m/z 367.

*2-{2-[(2S)-2-Methyl-2,3-dihydro-1H-indol-1-yl]-2-oxoethyl}-6-(morpholin-4-yl)pyrimidin-4(3H)-one (**28**) and 2-{2-[(2R)-2-Methyl-2,3-dihydro-1H-indol-1-yl]-2-oxoethyl}-6-(morpholin-4-yl)-pyrimidin-4(3H)-one (**29**).* These products were obtained by chiral chromatography separation of **24** (311 mg, 0.88 mmol) on a Chiralpak T304 20 μM chiral column (1080 g, 20 μM, 8/35 cm), eluent acetonitrile/isopropanol, 90/10; flow rate 185 mL/min. After purification, **28** (150 mg) was obtained, as first enantiomer, in the form of a pink amorphous solid. ^{1}H NMR (400 MHz): for this batch, the signals are broad; 1.26 (d, J = 6.8 Hz, 3H); 2.44 (m partially masked, 1H); 2.69 (d, J = 15.2 Hz, 1H); 3.42 (m, 4H); 3.60 (m, 4H); 3.72 (d, J = 15.7 Hz, 1H); 3.92 (d, J = 15.7 Hz, 1H); 4.72 (m, 1H); 5.20 (s, 1H); 7.04 (t, J = 7.8 Hz, 1H); 7.18 (t, J = 7.8 Hz, 1H); 7.28 (d, J = 7.8 Hz, 1H); 7.96 (d, J = 7.8 Hz, 1H); 11.67 (broad m, 1H). Mass spectrometry: method A; T_r (min) = 0.70; $[M + H]^+$ m/z 355; $[M - H]^-$ m/z 353. Optical rotation: αD = +65.0° ± 1.3 (c = 1.736 mg in 0.5 mL of methanol). Then the second enantiomer, **29** (143 mg), was obtained in the form of a white amorphous solid. ^{1}H NMR (400 MHz): for this batch, the signals are broad; 1.26 (d, J = 6.8 Hz, 3H); 2.45 (m partially masked, 1H); 2.69 (m, 1H); 3.41 (m, 4H); 3.61 (m, 4H); 3.72 (d, J = 15.7 Hz, 1H); 3.92 (d, J = 15.7 Hz, 1H); 4.70 (m, 1H); 5.20 (s, 1H); 7.04 (t, J = 7.8 Hz, 1H); 7.18 (t, J = 7.8 Hz, 1H); 7.28 (d, J = 7.8 Hz, 1H); 7.96 (d, J = 7.8 Hz, 1H); 11.64 (broad m, 1H). Mass spectrometry: method A; T_r (min) = 0.70; $[M + H]^+$ m/z 355; $[M - H]^-$ m/z 353. Optical rotation: αD = −72.8° ± 1.2 (c = 2.338 mg in 0.5 mL of methanol).

*4-Trifluoromethoxy-1H-indole, **30a**.* To a solution of of 4-(trifluoromethoxy)-1*H*-indole-2-carboxylic acid (3 g, 12.24 mmol) in 14 mL of quinolein, copper powder (0.54 g, 8.57 mmol) was added, and the reaction mixture was stirred at 200 °C for 5 h then cooled to room temperature. The mixture was diluted with 30 mL of diethyl ether and then filtered over Clarcel. The filtrate was washed successively with an aqueous 6 N HCl solution, a saturated aqueous solution of sodium bicarbonate, and brine. The organic layer was dried over magnesium sulfate, filtered, and concentrated under reduced pressure and then purified on silica gel (cyclohexane/ethyl acetate, 95/05) to give **30a** (1 g, 41%) as an amber oil. ^{1}H NMR (400 MHz): 6.48 (broad s, 1H); 6.96 (d, J = 7.9 Hz,

dx.doi.org/10.1021/jm401642q | J. Med. Chem. 2014, 57, 903−920

1H); 7.14 (t, J = 7.9 Hz, 1H); 7.41 to 7.47 (m, 2H); 11.49 (broad m, 1H). Mass spectrometry: method A; T_r (min) = 1.01; $[M - H]^-$ m/z 200.

4-Trifluoromethoxy-2,3-dihydro-1H-indole, ***31a.*** To a solution of **30a** (0.87 g, 4.32 mmol) in trifluoroacetic acid (12 mL) at −5 °C, sodium cyanoborohydride (0.57 g, 8.63 mmol) was added in portions, and the reaction mixture was stirred at 0 °C for 3 h. The mixture was poured into 60 mL of rapidly stirring ice water, and the solution was treated with concentrated NH_4OH to basic pH. After stirring for 30 min, the mixture was extracted with ethyl acetate, and the combined organic extracts were dried over magnesium sulfate, filtered, and concentrated in vacuo. The crude residue was purified on silica gel (cyclohexane/ethyl acetate, 95/05) to give **31a** as a yellow oil (0.18 g, 21%). Mass spectrometry: method A; T_r (min) = 0.81; $[M + H]^+$ m/z 204.

4-(4-Methylpiperazin-1-yl)-2,3-dihydro-1H-indole, ***31b.*** To a solution of 4-(4-methyl-piperazin-1-yl)-1*H*-indole[46] (490 mg, 2.28 mmol, **30b**) in acetic acid (17 mL), sodium cyanoborohydride (429 mg, 6.83 mmol) was added in portions, and the reaction mixture was stirred at room temperature for 2 h. The mixture was poured into 50 mL of rapidly stirring ice water, and the solution was made basic with concentrated NH_4OH. After stirring for 15 min, the mixture was extracted with dichloromethane, and the combined organic extracts were dried over magnesium sulfate, filtered, and concentrated in vacuo. The crude residue was purified on silica gel (DCM/MeOH, 95/05) to give **31b** (395 mg, 80%) as a colorless oil. ^{1}H NMR (400 MHz): 2.21 (s, 3H); 2.43 (m, 4H); 2.79 (t, J = 8.4 Hz, 2H); 2.88 (m, 4H); 5.30 (broad s, 1H); 6.15 (d, J = 7.9 Hz, 1H); 6.19 (d, J = 7.7 Hz, 1H); 7.11 (t, J = 7.9 Hz, 1H).

4-[(4-Methylpiperazin-1-yl)methyl]-2,3-dihydro-1H-indole, ***31c.*** To a solution 4-(4-methyl-piperazin-1-ylmethyl)-1*H*-indole[47,48] (1,58 g, 6.89 mmol, **30c**) in acetic acid (40 mL), sodium cyanoborohydride (1.3 g, 20.67 mmol) was added in portions, and the reaction mixture was stirred at room temperature for 2 h. The mixture was poured into 100 mL of rapidly stirring ice water, and the solution was made basic with concentrated NH_4OH. After stirring for 5 min, the mixture was extracted with dichloromethane. The combined organic extracts were dried over magnesium sulfate, filtered, and concentrated in vacuo. The crude residue was purified on silica gel (DCM/NH_3 7 N in MeOH, 95/05) to give **31c** (1.22 g, 76%) as a yellow powder. ^{1}H NMR (300 MHz): 2.13 (s, 3H); 2.19 to 2.31 (m, 4H); 2.89 (t, J = 8.6 Hz, 2H); 3.30 (s, 2H); 3.31 to 3.44 (m, 6H); 5.37 (broad s, 1H); 6.37 (d, J = 7.7 Hz, 1H); 6.44 (d, J = 7.7 Hz, 1H); 6.83 (t, J = 7.7 Hz, 1H).

In Vitro PI3K Enzyme Assay. Human p110α and δ with N-terminal poly-His tags were coexpressed with p85α in a Sf9 baculovirus expression system, and the p110α and -δ/p85α heterodimers were purified by sequential Ni-NTA and heparin chromatography. Human p110β with an N-terminal poly-His tag was coexpressed with p85α in a S21 baculovirus expression system, and the p110β/p85α heterodimer was purified by sequential Ni-NTA, A-EX (Q-HP), and Superdex S200 chromatography. A truncated form of human PI3Kγ encompassing residues Ser144−Ala1102, C-terminally labeled with a poly-His tag, was expressed with baculovirus in Sf9 insect cells and purified by sequential Ni-NTA and Superdex-200 chromatography. Lipid kinase activity assays were performed using PI3K HTRF (homogeneous time-resolved fluorescence) Millipore kit in 384 well format according to manufacturer instructions. The assay was performed in 10 μL reaction volume: serial dilutions of inhibitors (3% DMSO) were preincubated for 15 min at room temperature (RT) with 10 μM PI(4,5)P2 substrate/enzyme mixture before starting the reaction by the addition of 100 μM ATP. Enzyme concentrations correspond to 100, 15, 30, and 400 pM for α, β, δ, and γ isoforms, respectively. After 15 min incubation at RT, the enzymatic reaction was stopped, and the revelation mixture added (Millipore kit). The signals of fluorescence at 665 and 620 nm were recorded after O/N incubation at 4 °C. The results were expressed as fluorescence signal ratio ((665/620) × 10000). For this competition binding assay, wells without enzyme were used to calculate the maximal signal (max). The nontreated wells containing 3% DMSO were used to determine the minimum signal (min). The percentage inhibition was calculated for each concentration of compound according to the following formula:

$$\%\ \text{inhibition} = 100 \times \left[\frac{(\text{signal ratio test} - \text{signal ratio min})}{(\text{signal ratio max} - \text{signal ratio min})}\right]$$

The activity of the product was estimated by using the concentration of compound where percent inhibition is equal to 50 (IC_{50}) obtained from a dose−response curve with 11 concentrations tested in single replicates and fitted with XLFit 4 software from Excel version 4.2.2 using the four-parameter logistic model (eq 205). IC_{50} values represent the mean from at least two independent experiments.

Cell Based Akt Phosphorylation Assays. All parental cell lines were purchased from ATCC.[49] Cells were cultured in DMEM high glucose medium, except for BT549, which was cultured in RPMI1640 medium, containing 10% fetal calf serum and 2 mM glutamine (complete culture medium).

MEF/3T3-Myristoylated p110β cell line was an inducible stable clone established by transfecting a pTRE2Hygro-myc vector and human myr wt PI3KCB sequence of interest in mouse embryonic fibroblast MEF3T3 Tet Off (Clontech 631139). Cells were cultured in DMEM high glucose medium supplemented with 10% tet system approved FCS, 2 mM L-glutamine, 100 μg/mL Geneticin, 200 μg/mL hygromycin B.

MEF/3T3-Myristoylated p110δ cell line was an inducible stable clone established by transfecting a pTRE2Hygro-myc vector and human myr wt PI3KCD sequence of interest in mouse embryonic fibroblast MEF3T3 Tet Off (Clontech 631139). Cells were cultured in the same medium as described for MEF/3T3-myristoylated p110β.

The Akt phosphorylation assay was based on a sandwich immunoassay using the MSD Multispot biomarker detection kit from Meso Scale Discovery "phospho-Akt (Ser473) whole cell lysate kit" (no. K151CAD) . The primary antibody specific for Akt was coated onto an electrode in each well of the 96-well plates of the MSD kit. After the addition of a protein lysate to each well, the signal was visualized by adding a secondary detection antibody specific for pAkt-S473 and labeled with an electrochemiluminescent compound. The procedure followed was that described in the MSD kit. On day 1, cells were seeded into 96-well plates at the concentration of 5000 to 35000 cells/well depending on the cell line (PC3, LnCaP, MDA-MB-468, BT549, H460, and U87-MG cells), 20000 cells/well (MEF/3T3-myristoylated p110δ and MEF/3T3-Myristoylated p110β cells), or 320000 cells/well (Raw 264.7 cells) in 200 μL of DMEM complete medium (PC3, MEF/3T3-myristoylated p110β and MEF/3T3-myristoylated p110δ cells) or in serum-free medium (Raw 264.7 cells) and incubated at 37 °C, overnight, in the presence of 5% CO_2. On day 2, cells were incubated in the presence or absence of the test products for 30 min to 2 h at 37 °C in the presence of 5% of CO_2. In the case of Raw 264.7, at the end of compound treatment, cells were stimulated for 5 min with complement protein C5a at 10^{-8} M final concentration at 37 °C in the presence of 5% of CO_2. In the case of MEF/3T3-myristoylated p110δ, cells were serum-deprived for 6 h before treatment with test compounds in serum-free medium. The molecules, diluted in dimethyl sulfoxide, were added from a 20-fold concentrated stock solution, the final DMSO concentration being 0.1%. The molecules were tested either at a single concentration of less than or equal to 10 μM, or at increasing concentrations ranging from less than 1 nM to 10 μM. After incubation, cells were lysed for the preparation of the proteins, according to the MSD kit description. The plates were read on the S12400 instrument from Meso Scale Discovery. Wells without cells and containing the lysis buffer were used to determine the background noise that will be subtracted from all the measurements (min). The wells containing cells in the absence of product and in the presence of 0.1% DMSO were used to determine the 100% signal (max). The IC_{50} values represent the mean from two independent experiments.

The Akt (Thr 308) phosphorylation cell based assay was conducted under the same conditions but replacing the secondary antibody specific for pAkt-S473 with the secondary antibody specific for pAkt-T308 (MSD kit no. K151DYD).

In Vivo Studies. *Pharmacokinetic Assays. In Mice.* Balb/c female mice were used for the 3 mg iv and 10 mg and 100 mg po experiments.

dx.doi.org/10.1021/jm401642q | J. Med. Chem. 2014, 57, 903−920

Mice were fed ad libitum, and compound **28** was administered using the following formulations: intravenous route, 3 mg of compound **28** was dissolved in 50 μL of ethanol and 50 mg of Tween 80 under stirring, until complete dissolution, and solution was completed up to 1 mL using dextrose 5%; oral route, 2 mg (or 20 mg) of compound **28** was added to 125 μL of ethanol and 125 mg of Tween 80 under stirring, until complete dissolution, and solution was completed up to 1 mL using dextrose 5%. Twenty-four mice were used for each route (three mice per time point, 0.083 h (iv), 0.25 h (po), 0.5 h, 1 h, 2 h, 4 h, 6 h, 8 h, and 24 h); blood samples were collected and transferred into eppendorf tubes containing lithium heparin as anticoagulant. After centrifugation (1500*g* for 10 min at 4 °C), plasma samples were frozen at a temperature close to −20 °C, and compound **28** was quantified by LC/MS-MS. Quality control samples and calibration samples were prepared by spiking mice plasma with working solutions prepared from independent weightings. The QC-sample concentrations were adjusted to theoretical values of 1.5, 225, and 450 ng/mL. The calibration curve was calculated from theoretical calibration levels of 1 (n = 3), 5, 10, 50, 100, 250, and 500 ng/mL (n = 3) weighed by $1/x$ using a linear regression not forced through the origin. The lower limit of quantitation (LLOQ) was 1 ng/mL. Pharmacokinetic modeling and analysis were performed with WinOnLine 5.2 software using noncompartmental model.

In Rats. Bioavailability of compound **28** following single oral (10 mg/kg) or intravenous (3 mg/kg) administration to female Nude rats was performed using the same protocols as for the mice (*vide supra*).

In Dogs. Bioavailability of compound **28** following single oral (10 mg/kg) or intravenous (3 mg/kg) administration to male Beagle dogs was performed using the same protocols as for the mice (*vide supra*), with the difference that in both formulations the polysorbate (Tween 80) was replaced with solutol.

PD Assay. For PK/PD studies, animals bearing tumors were randomized according to a given median tumor burden range on a specific day post-tumor implantation, and treatment was administered as indicated with three animals per group. At designated time points posttreatment as indicated, mice were anesthetized and euthanized, and blood samples were collected and kept for PK analysis. Tumors were resected, frozen in dry ice in small fragments in screw-capped tubes containing 2.8 mm ceramic beads (Ozyme no. BER1030), and stored at −80 °C until use. Protein extracts were prepared in lysis buffer [10 mM Tris, pH 7.5 (InVitrogen no. 15567-027), 100 mM NaCl (Sigma no. S5150), 1 mM EDTA, pH 8 (InVitrogen no. 15575-038), 1 mM EGTA, pH 8 (Sigma no. E4378), 1% Triton (Sigma no. T9284), 1 mM NaF (Sigma no. S7920), 20 mM $Na_4P_2O_7$ (Sigma no. S6422), 1 mM activated Na_3VO_4 (Sigma no. S6508), and 10% glycerol (Fisher Scientific no. G/0650/17) supplemented with protease inhibitor mix (Roche no. 11836145001)] by mechanical dissociation using the Precellys 24 bead beating homogenizer (Ozyme, no. BER1011) set at two runs of 2 × 30 s at 6000 rpm at 4 °C and connected to a Cryolys cooling system. The extracts were incubated 2 h at 4 °C to extract membrane proteins and clarified by a 16000*g* centrifugation for 15 min at 4 °C, and supernatants were collected, aliquoted, snap frozen in dry ice, and stored at −80 °C until analysis.

Protein concentrations were determined by the Bradford method (kit Pierce BCA 23225) according to the manufacturer instructions. Tumor extract samples were not diluted for the assays. Levels of total AKT protein and phospho proteins pAkt-S473 and pAkt-T308 were determined using Mesoscale electrochemiluminescence duplex immunoassays according to manufacturer instructions. The impact on biomarker upon compound treatment was expressed as the mean modulation of target kinase phosphorylation in treated tumors compared with the vehicle tumors and was calculated as [(mean phospho/total protein for treated group)/(mean phospho/total protein for vehicle group) × 100] − 100.

Xenograft Studies. Human prostate PC-3 and melanoma UACC-62 cells were purchased at ATCC (batch CTRL-1435, Rockville, MD, USA) and at NCI (batch 0503000, DTP/DCTD/NCI1003 W. Seventh Street, Frederick, MD USA 21701-8531), respectively. The PC-3 was initiated from a bone metastasis of grade V prostatic adenocarcinoma from a 62-year-old male Caucasian. PC3 cells were cultured in F-12 medium containing 10% fetal calf serum (FCS) and 2 mL of glutamine, and UACC-62 cells were cultured in RPMI1640 medium supplemented with 10% FBS and 2 mM L-glutamine. PC3 and UACC-62 tumor models were established by implanting subcutaneously (sc) 3×10^6 cells mixed with 50% matrigel (reference 356234, Becton Dickinson Biosciences) per SCID female mouse and were maintained by sc serial passages once every 3 weeks in SCID female mice. Animals bearing tumors were randomized according to a given median tumor burden range on a specific day post-tumor implantation, and the compound was administered orally at the indicated dose twice a day (bid) in solution in the following formulation: 12.5% ethanol/12.5% polysorbate 80/75% isotonic glucose 5% in water, pH 2) for both studies, with seven animals per group. Tumor volume was measured regularly during the treatment period. Changes in tumor volume for each treated (T) and control (C) group were calculated for each tumor by subtracting the tumor volume on the day of first treatment (staging day) from the tumor volume on the specified observation day. The median ΔT was calculated for the treated group, and the median ΔC was calculated for the control group. Then the ratio $\Delta T/\Delta C$ was calculated and expressed as a percentage. The dose was considered as therapeutically active when $\Delta T/\Delta C$ was lower than 40%.[50] For statistical analysis, a two-way ANOVA with repeated measures was applied to the ranks of the tumor volume changes from baseline (TVday − TV0) and (CVday − CV0), followed by a Winer analysis at each day of tumor measurement. In case of significance, a Dunnett's test was performed versus control. Statistical analyses were performed on SAS system release 8.2 for SUN4 via Everstat V5 software and SAS 9.2 software. A probability less than 5% ($p < 0.05$) was considered as significant.

Crystallography. *Determination of Compound 7 Crystal Structure from X-ray Single-Crystal Diffraction Data.* Crystal data for compound **7** was collected at T = 298(2) K on a Bruker AXS 3-circle Smart-APEX diffractometer (χ-axis fixed at 54.748°) running on Smart v5.634 program (Bruker AXS, Madison, WI, USA, 2009). A sealed molybdenum anode X-ray tube (Mo Kα line, λ = 0.710731 Å) was used, running at 50 kV and 40 mA. To reduce the extraneous Kβ radiation, a graphite crystal monochromator was inserted in the incident beam path just after the safety shutter. In addition, a 0.5 mm MonoCap optical fiber collimator was used to increase the output flux that strikes the sample. A charge-coupled device (CCD chip, 4 K, 62 mm) area detector positioned at 6.0 cm completed the setup. The crystal was selected under an optical microscope (approximate crystal dimensions: 100 × 200 × 300 μM^3) and then glued with Araldite onto a quartz rod. A full Ewald sphere of reflections was collected (3 × 600 frames, applying ω-scans with step widths of 0.3°). Accumulation time was set at 60 s for each frame to be acquired. The orientation matrix and unit cell were established using the SMART v5.634 program. The 3D reflection profile and the integration of all reflections were done with the SAINT+ v6.45 program (Bruker AXS, Madison, WI, USA, 2003). The SADABS v2.10 program (Bruker AXS, Madison, WI, USA, 2003) was then used for reflection scaling and for Lorentz, polarization, and absorption effects correction. The tentative space group was determined with the XPREP v6.14 program (Bruker AXS, Madison, WI, USA, 2003). The SHELXTL v6.14 program suite (Bruker AXS, Madison, WI, USA, 2003) was then applied to solve the structure by direct methods. All non-hydrogen atoms were refined anisotropically using full-matrix least-squares refinement on F^2. All hydrogen atoms have been located on Fourier difference map and subsequently included in the refinement.

CCDC 946768 contains the supplementary crystallographic data for this paper. These data can be obtained free of charge from The Cambridge Crystallographic Data Centre via www.ccdc.cam.ac.uk/data_request/cif.

Determination of p110β Crystal Structure. Mouse p110β (114−1064) was expressed and purified following published procedures for mouse p110δ.[36] The protein crystallized in the presence of 1.7 M of NaCl in 100 mM Hepes buffer, pH 7, at 20 °C and a solution of crystal seeds diluted to 1/7500. Crystal seeds were obtained by crystallizing the protein in the presence of 14−16% PEG

Table 8. Crystal Data and Structure Refinement for Compound 7

CCDC code	946768
empirical formula	$C_{18}H_{20}N_4O_3$
formula weight	340.38
temp	298(2) K
cryst syst	monoclinic
space group	$P2_1/n$
a	6.3721(5) Å
b	24.135(2) Å
c	10.9429(9) Å
β	96.1460(10)°
vol	1673.2(2) Å^3
Z	4
ρ_{calc}	1.351 g/cm^3
μ	0.095 mm^{-1}
F(000)	720.0
2Θ range for data collection	3.38°−46.58°
index ranges	$-7 \le h \le 7$, $-26 \le k \le 26$, $-12 \le l \le 11$
data set completeness	100%
reflns measured	10161
unique reflns	2407 (Rint = 2.8%)
data/restraints/params	2407/0/307
GOF on F^2	1.078
final R indexes [$I \ge 2\sigma(I)$]	R_1 = 0.0444, wR_2 = 0.1043
final R indexes [all data]	R_1 = 0.0605, wR_2 = 0.1119
largest diff. peak/hole	0.15/−0.14 e Å^{-3}

Table 9. X-ray Data Collection and Refinement Statistics for Compound 28[a]

Data Collection	
space group	$P2_12_12_1$
unit cell dimensions	
a, b, c (Å)	122.3, 129.0, 154.9
α, β, γ (deg)	90.0, 90.0, 90.0
resolution (Å)	154.9−2.8 (2.87−2.80)
total reflns	360129
unique reflns	60910
completeness (%)	99.8 (100)
Rsym	8.7 (126.9)
$I/\sigma(I)$	17.8 (1.3)
Refinement	
reflns used	60840
R_{free}/R	27.5/26.0
average B-values (Å^2)	76.9
number of atoms	
protein	**13645**
ligand	132
solvent	80
rms deviations	
bond lengths (Å)	0.008
bond angles (deg)	0.87

[a]Data in parentheses correspond to the highest resolution shells. To calculate R_{free}, 5% of the reflections were excluded from the refinement. R_{sym} is defined as $R_{sym} = \sum_{hkl}\sum_i|I_i(hkl) - \langle I(hkl)\rangle|/\sum_{hkl}\sum_i I_i(hkl)$. The highest resolution shell cutoff was defined using the correlation coefficient between random half-data sets $CC_{1/2}$ = 0.5 as described in *POINTLESS*.[55]

8000, 28−32% ethylene glycol, and 100 mM carboxylic acids in 100 mM Mes/imidazole buffer, pH 6.5. Co-crystals were obtained by mixing 1 μL of protein (8 mg/mL), 1 mM compound **28**, and 1 μL of precipitant with 0.2 μL of the diluted seeding solution. Crystals were flash-frozen in liquid nitrogen prior to data collection. Diffraction data for p110β−compound **28** were collected at the Swiss LightSource, beamlinePXIII, using λ = 1.0 Å and a Pilatus 2M detector. Data were processed using autoPROC,[51] and the structure was solved by molecular replacement using MOLREP[52] using the mouse p110β structure as the search model (PDB code 2Y3A). The structure was refined using BUSTER/TNT,[53] and model building was performed with COOT.[54] Coordinates and structure factors were deposited at the Protein Data Bank under the code 4BFR.

AUTHOR INFORMATION

Corresponding Author

*Telephone: +33(0)1 58 93 36 14. Fax: +33(0)1 58 93 80 14. E-mail: frank.halley@sanofi.com.

Notes

The authors declare no competing financial interest.

ACKNOWLEDGMENTS

We thank Serge Sablé, Frédéric Herman, Bertrand Monegier, and Fabrice Debu and their respective teams for structural analyses. We thank Jean-Pascal Ridoux for physicochemical studies, Olivier Courtin for Caliper binding assay studies, and Odile Angouillant, Pierre-Eric Bardouillet, Eric Brohan, Pascal Collemine, and Celine Prévost for chiral separations. We thank Véronique Lalleman, Marie-France Bachelot, Christelle Castell, and Françoise Begassat for biochemical assays. We thank Agnès Vergezac, Laurent Bassinet, Virginie Boisrobert, Laurent Dassencourt, Françoise Hervé, Alexandre Rohaut, Anne Thomas, Yvette Ruffin, Frédéric Foucault, and Chagri Boumaya for their technical assistance. We thank Alain Krick, Valerie Czepczor, Carole Deshayes, Madeleine Coimbra, Cecile Ducelier, Virginie Panek, Anne-Laure Coutant, Stephane Muccio, and Anne Perreard-Dumaine for in vitro pharmacokinetic studies and Gary McCort for his thorough proof-reading of the manuscript.

ABBREVIATIONS USED

ADME, adsorption, distribution, metabolism, and excretion; Akt, protein kinase B PKB; BID, bis in die (twice a day); ATM, ataxia telangiectasia mutated; ATR, ataxia telangiectasia and Rad3 related; DCM, dichloromethane; DIPEA, diisopropyl ethyl amine; DMF, *N*,*N*-dimethylformamide; DMSO, dimethyl sulfoxide; DNA-PK, DNA-dependent protein kinase; EC, effective concentration; EDCI, 1-ethyl-3-(3-(dimethylamino)-propyl)carbodiimide; HLM, human liver microsomes; IC_{50}, inhibitory concentration at half maximal effect; iv, intravenous; LE, ligand efficiency; mTOR, mammalian target of rapamycin; pAkt, phospho serine−threonine kinase Akt; PD, pharmacodynamic; PDK1, phosphoinositide-dependent kinase-1; PI3K, phosphoinositide 3-kinase; PK, pharmacokinetic; PIP2, phosphatidylinositol-4,5-bisphosphate; PIP3, phosphatidylinositol-3,4,5-trisphosphate; po, per os (orally); PTEN, phosphatase and tensin homologue gene; qd, quaque die (once a day); rat sarcoma, RAS; rmsd, root-mean-square deviation; SAR, structure−activity relationship; SBE-β-cyclodextrin, sulfobutyl ether β-cyclodextrin; SCID, severe combined immunodeficiency; TFA, trifluoroacetic acid; THF, tetrahydrofuran; Xantphos, 4,5-bis(diphenylphosphino)-9,9-dimethylxanthene

REFERENCES

(1) Engelman, J. A.; Luo, J.; Cantley, L. C. The evolution of phosphatidylinositol 3-kinases as regulators of growth and metabolism. *Nat. Rev. Genet.* **2006**, *7*, 606−619.

(2) Hirsch, E.; Braccini, L.; Ciraolo, E.; Morello, F.; Perino, A. Twice upon a time: PI3K's secret double life exposed. *Trends Biochem. Sci.* **2009**, *34*, 244−248.

(3) Courtney, K. D.; Corcoran, R. B.; Engelman, J. A. The PI3K pathway as drug target in human cancer. *J. Clin. Oncol.* **2010**, *28*, 1075−1083.

(4) Yuan, T. L.; Cantley, L. C. PI3K pathway alterations in cancer: Variations on a theme. *Oncogene* **2008**, *27*, 5497−5510.

(5) Liao, Y.; Hung, M. C. Physiological regulation of Akt activity and stability. *Am. J. Transl. Res.* **2010**, *2*, 19−42.

(6) Ihle, N. T.; Powis, G. The biological effects of isoform-specific PI3-kinase inhibition. *Curr. Opin. Drug Discovery Dev.* **2010**, *13*, 41−49.

(7) Ward, S. G.; Finan, P. Isoform-specific phosphoinositide 3-kinase inhibitors as therapeutic agents. *Curr. Opin. Pharmacol.* **2003**, *3*, 426−434.

(8) Wee, S.; Wiederschain, D.; Maira, S.-M.; Loo, A.; Miller, C.; deBeaumont, R.; Stegmeier, F.; Yao, Y.-M.; Lengauer, C. PTEN-deficient cancers depend on PIK3CB. *Proc. Natl. Acad. Sci. U.S.A.* **2008**, *105*, 13057−1362.

(9) Jia, S.; Liu, Z.; Zhang, S.; Liu, P.; Zhang, L.; Hyun, S.; Zhang, L. J.; Signoretti, S.; Loda, M.; Roberts, T. M.; Zhao, J. J. Essential roles of PI(3)K−p110β in cell growth, metabolism and tumorigenesis. *Nature* **2008**, *45*, 776−779.

(10) Kim, J.; Hong, S.; Hong, S. Discovery of new aminopyrimidine-based phosphoinositide 3-kinase beta (PI3Kβ) inhibitors with selectivity over PI3Kα. *Bioorg. Med. Chem. Lett.* **2011**, *21*, 6977−6981.

(11) Hardwicke, M. A.; Ariazi, J.; Bushdid, P.; Erhard, K.; McSurdy-Freed, J.; Lin, H.; Luengo, J.; Mack, J.; Pietrak, B.; Plant, R.; Qu, J.; Raha, K.; Rominger, C.; Sanchez, R. M.; Schaber, M. D.; Schulz, M. J.; Sherk, C.; Sinnamon, R.; Skordos, K.; Spengler, M.; Squire, M.; Tedesco, R.; Xie, R.; Yu, H.; Zeng, J.; Rivero, R. A. Presented at the 243rd ACS National Meeting, San Diego, CA, March 25−29, 2012. Abstract MEDI 21.

(12) Hardwicke, M. A.; Rivero, R. A. Presented at the AACR 103rd Annual Meeting, Chicago March 31 - April 4, 2012. Abstract Number 2913.

(13) Lin, H.; Erhard, K.; Hardwicke, M. A.; Luengo, I. L.; Mack, J. F.; McSurdy-Freed, J.; Plant, R.; Raha, K.; Rominger, C.; Sanchez, R. M.; Schaber, M. D.; Schulz, M. J.; Spengler, M. D.; Tedesco, R.; Xie, R.; Zeng, J. J.; Rivero, R. A. Synthesis and structure−activity relationships of imidazo[1,2-a]pyrimidin-5(1H)-ones as a novel series of beta isoform selective phosphatidylinositol 3-kinase inhibitors. *Bioorg. Med. Chem. Lett.* **2012**, *22*, 2230−2234.

(14) (a) Sanchez, R. M.; Erhard, K.; Hardwicke, M. A.; Lin, H.; McSurdy-Freed, J.; Plant, R.; Raha, K.; Rominger, C. M.; Schaber, M. D.; Spengler, M. D.; Moore, M. L.; Yu, H.; Luengo, J. L.; Tedesco, R.; Rivero, R. A. Synthesis and structure-activity relationships of 1,2,4-triazolo[1,5-a]pyrimidin-7(3H)-ones as novel series of potent β isoform selective phosphatidylinositol 3-kinase inhibitors. *Bioorg. Med. Chem. Lett.* **2012**, *22*, 3198−3202. (b) Lin, H.; Schulz, M. J.; Xie, R.; Zeng, J.; Luengo, J. I.; Squire, M. D.; Tedesco, R.; Qu, J.; Erhard, K. F.; Mack, J. F.; Raha, K.; Plant, R.; Rominger, C. M.; Ariazi, J. L.; Sherk, C. S.; Schaber, M. D.; McSurdy-Freed, J.; Spengler, M. D.; Davis, C. B.; Hardwicke, M. A.; Rivero, R. A. Rational design, synthesis, and SAR of a novel thiazolopyrimidinone series of selective PI3K-beta inhibitors. *ACS Med. Chem. Lett.* **2012**, *3*, 524−529.

(15) Yu, H.; Moore, M. L.; Erhard, K.; Hardwicke, M. A.; Lin, H.; Luengo, J. I.; McSurdy-Freed, J.; Plant, R.; Qu, J.; Raha, K.; Rominger, C. M.; Schaber, M. D.; Spengler, M. D.; Rivero, R. A. [3a,4]-Dihydropyrazolo[1,5a]pyrimidines: Novel, potent, and selective phosphatidylinositol-3-kinase β inhibitors. *ACS Med. Chem. Lett.* **2013**, *4* (2), 230−234.

(16) Hancox, U.; Cosulich, S.; Dry, H.; Hanson, L.; Trigwell, C.; Crafter, C.; Barlaam, B.; Plé, P.; Fitzek, M.; Wedge, S.; Ward, L.; Powel, S.; Ellston, R.; Lawson, M.; Harrington, L.; Cumberbatch, M.; Green, S.; Barry, S. AZD8186: A potent selective inhibitor of PI3Kβ targeting PTEN-deficient tumours dependent on dysregulated PI3Kβ signalling. Presented at the AACR 104th Annual Meeting, Washington DC, April 6−12, 2013. Poster Number 3264.

(17) Carry, J.-C.; Certal, V.; Halley, F.; Karlsson, K. A.; Schio, L.; Thompson, F. Novel [4-(morpholin-4-yl)-6-oxo-1,6-dihydropyrimidin-2-yl]amide derivatives, their preparation, their pharmaceutical compositions and their use as AKT(PKB) phosphorylation inhibitors for treating cancers. PCT Int. Appl. WO2011001114, 2011.

(18) Certal, V.; Halley, F.; Virone-Oddos, A.; Thompson, F.; Filoche-Rommé, B.; El-Ahmad, Y.; Carry, J. C.; Delorme, C.; Karlsson, A.; Abecassis, P. Y.; Bonnevaux, H.; Nicolas, J. P.; Morales, R.; Michot, N.; Vade, I.; Louboutin, A.; Perron, S.; Doerflinger, G.; Tric, B.; Monget, S.; Lengauer, C.; Schio, L. Preparation and optimization of new 4-(morpholin-4-yl)- (6-oxo-1,6-dihydropyrimidin-2-yl)amide derivatives as PI3Kβ inhibitors. *Bioorg. Med. Chem. Lett.* **2012**, *22*, 6381−6384.

(19) Certal, V.; Halley, F.; Virone-Oddos, A.; Delorme, C.; Karlsson, A.; Rak, A.; Thompson, F.; Filoche-Rommé, B.; El-Ahmad, Y.; Carry, J. C.; Abecassis, P. Y.; Lejeune, P.; Vincent, L.; Bonnevaux, H.; Nicolas, J. P.; Bertrand, T.; Marquette, J. P.; Michot, N.; Benard, T.; Below, P.; Vade, I.; Chatreaux, F.; Pilorge, F.; Angouillant Boniface, O.; Louboutin, A.; Lengauer, C.; Schio, L. Discovery and optimization of new benzimidazole- and benzoxazole-pyrimidone selective pi3kβ inhibitors for the treatment of phosphatase and tensin homologue (PTEN)-deficient cancers. *J. Med. Chem.* **2012**, *55*, 4788−4805.

(20) Hopkins, A. L.; Groom, C. R.; Alex, A. Ligand efficiency: A useful metric for lead selection. *Drug Discovery Today* **2004**, *9*, 430−431.

(21) Jackson, S.; Schoenwaelder, S.; Goncalves, I.; Nesbitt, W.; Yap, C. L.; Wright, C. E.; Kenche, V.; Anderson, K. E.; Dopheide, S. M.; Yuan, Y.; Sturgeon, S. A.; Prabaharan, H.; Thompson, P.; Smith, G. D.; Shepherd, P. R.; Daniele, N.; Kulkarni, S.; Abbott, B.; Saylik, D.; Jones, C.; Lu, L.; Giuliano, S.; Hughan, S. C.; Angus, J. A.; Robertson, A. D.; Salem, H. H. PI3-kinase p110β: A new target for antithrombotic therapy. *Nat. Med.* **2005**, *11*, 507−514.

(22) Leroux, F. R.; Manteau, B.; Vors, J.-P.; Pazenok, S. Trifluoromethyl ethers−synthesis and properties of an unusual substituent. *Beilstein J. Org. Chem.* **2008**, *4*, 1−15 and references therein.

(23) Equilibrated solubility protocol: 1 mg of solid was mixed with 500 μL of 50 mM phosphate buffer at pH 7.4 (prepared by mixing 40.5 mL of a 0.1 M dibasic sodium phosphate stock solution with 9.5 mL of a 0.1 M monobasic sodium phosphate stock solution, and adding 50 mL of water), and the suspension was set on a bottle roller at 60 rpm for 16 h at ambient temperature. The mixture was then filtered, and the solution was analyzed by HPLC for quantization.

(24) Ran, Y.; He, Y.; Yang, G.; Johnson, J. L. H.; Yalkowsky, S. H. Estimation of aqueous solubility of organic compounds by using the general solubility equation. *Chemosphere* **2002**, *48*, 487−509.

(25) Ishikawa, M.; Hashimoto, Y. Improvement in aqueous solubility in small molecule drug discovery programs by disruption of molecular planarity and symmetry. *J. Med. Chem.* **2011**, *54*, 1539−1554.

(26) Mitchell, A. G. Racemic drugs: Racemic mixture, racemic compound, or pseudoracemate? *J. Pharm. Pharm. Sci.* **1998**, *1*, 8−12.

(27) Caroa, I.; Boulenca, X.; Roussetb, M.; Meuniera, V.; Bourriéa, M.; Juliana, B.; Joyeux, H.; Roquesa, C.; Bergera, Y.; Zweibaumb, A.; Fabre, G. Characterisation of a newly isolated Caco-2 clone (TC-7), as a model of transport processes and biotransformation of drugs. *Int. J. Pharm.* **1995**, *116*, 147−158.

(28) Waring, M. L. Lipophilicity in drug discovery. *Expert Opin. Drug Discovery* **2010**, *5*, 235−248 and references therein.

(29) Alex, A.; Millan, D. S.; Perez, M.; Wakenhut, F.; Whitlock, G. A. Intramolecular hydrogen bonding to improve membrane permeability and absorption in beyond rule of five chemical space. *Med. Chem. Commun.* **2011**, *2*, 669−674 and references therein.

(30) Guimarães, C. R. W.; Mathiowetz, A. M.; Shalaeva, M.; Goetz, G.; Liras, S. Use of 3D properties to characterize beyond rule-of-5 property space for passive permeation. *J. Chem. Inf. Model.* **2012**, *52*, 882−890.

(31) Gleeson, M. P. Generation of a set of simple, interpretable ADMET rules of thumb. *J. Med. Chem.* **2008**, *51*, 817−834.
(32) Caliper-based assay on 192 kinases: 79 RTK, 3 STK, 11 STE, 6 CK1, 29 AGC, 37 CAMK, 20 CGMC, 7 atypical. After a preincubation time of 15 min between the enzyme and the inhibitor, the enzymatic incubations are performed at 28 °C during 90 min in a phosphate buffer at pH 7.4 containing 1 mM DTT, then stopped by EDTA addition. Compound **8** was tested over three concentrations (0.1, 1, and 10 μM).
(33) Zhang, X.; Vadas, O.; Perisic, O.; Anderson, K. E.; Clark, J.; Hawkins, P. T.; Stephens, L. R.; Williams, R. L. Structure of lipid kinase p110b/p85b elucidates an unusual SH2-domain-mediated inhibitory mechanism. *Mol. Cell* **2011**, *41*, 567−578.
(34) Walker, E. H.; Pacold, M. E.; Perisic, O.; Stephens, L.; Hawkins, P. T.; Wymann, M. P.; Williams, R. L. Structural determinants of phosphoinositide 3-kinase inhibition by wortmannin, LY294002, quercetin, myricetin, and staurosporine. *Mol. Cell* **2000**, *6*, 909−919.
(35) Knight, Z. S.; Chiang, G. G.; Alaimo, P. J.; Kenski, D. M.; Ho, C. B.; Coan, K.; Abraham, R. T.; Shokat, K. M. Isoform-specific phosphoinositide 3-kinase inhibitors from an arylmorpholine scaffold. *Bioorg. Med. Chem.* **2004**, *12*, 4749−4759.
(36) Berndt, A.; Miller, S.; Williams, O.; Le, D. D.; Houseman, B. T.; Pacold, J. I.; Gorrec, F.; Hon, W.-C.; Ren, P.; Rommel, C.; Gaillard, P.; Rückle, T.; Schwartz, K. M.; Shokat, K. M.; Shaw, J. P.; Williams, R. L. The p110? structure: mechanisms for selectivity and potency of new PI(3)K inhibitors. *Nat. Chem. Biol.* **2010**, *6*, 117−124.
(37) Knight, Z. S.; Gonzalez, B.; Feldman, M. E.; Zunder, E. R.; Goldenberg, D. D.; Williams, O.; Loewith, R.; Stokoe, D.; Balla, A.; Toth, B.; Balla, T.; Weiss, W. A.; Williams, R. L.; Shokat, K. M. A pharmacological map of the PI3-K family defines a role for p110α in insulin signaling. *Cell* **2006**, *125*, 733−747.
(38) Hon, W. C.; Berndt, A.; Williams, R. L. Regulation of lipid binding underlies the activation mechanism of class IA PI3-kinases. *Oncogene* **2012**, *31*, 3655−3666.
(39) Zheng, Z.; Miller, M. S.; Jennings, I. G.; Thompson, P. E. Mechanisms of PI3Kβ-selective inhibition revealed by reciprocal mutagenesis. *ACS Chem. Biol.* **2013**, *8*, 679−683.
(40) Nathanson, K. L.; Martin, A.-M.; Wubbenhorst, B.; Greshock, J.; Letrero, R.; D'Andrea, K.; O'Day, S.; Infante, J. R.; Falchook, G. S.; Arkenau, H.-T.; Millward, M.; Brown, M. P.; Pavlick, A.; Davies, M. A.; Ma, B.; Gagnon, R.; Curtis, M.; Lebowitz, P. F.; Kefford, R.; Kefford; Long, G. V. Tumor genetic analyses of patients with metastatic melanoma treated with the BRAF inhibitor dabrafenib (GSK2118436). *Clin. Cancer Res.* **2013**, *19* (17), 4868−4878.
(41) Kopetz, S.; Desai, J.; Chan, E.; Hecht, J. R.; O'Dwyer, P. J.; Lee, R. J.; Nolop, K. B.; Saltz, L. PLX4032 in metastatic colorectal cancer patients with mutant BRAF tumors. *J. Clin. Oncol.* **2010**, *28* (15s), 3534.
(42) Corcoran, R. B.; Ebi, H.; Turke, A. B.; Coffee, E. M.; Nishino, M.; Cogdill, A P.; Brown, R. D.; Della Pelle, P.; Dias-Santagata, D.; Hung, K. E.; Flaherty, K. T.; Piris, A.; Wargo, J. A.; Settleman, J.; Mino-Kenudson, M.; Engelman, J. A. EGFR-mediated reactivation of MAPK signaling contributes to insensitivity of BRAF-mutant colorectal cancers to RAF inhibition with vemurafenib. *Cancer Discovery* **2012**, *2* (3), 227−235.
(43) Garcia-Echeverria C.; Vincent, L.; Virone-Oddos, A. Compositions And Methods For Treating Cancer Using PI3Kβ Inhibitor and MAPK Pathway Inhibitor, Including Mek And Raf Inhibitors. PCT Int. Appl. WO2013037943, 2013.
(44) Virone-Oddos, A. Discovery and characterization of SAR260301, a novel PI3Kβ-selective inhibitor in clinical development for the treatment of PTEN-deficient tumors. Presented at the AACR 104th Annual Meeting, Washington DC April 6−12, 2013. Poster Number 3258.
(45) Halley, F. Discovery and optimization of new pyrimidone PI3Kb inhibitors for the treatment of PTEN-deficient cancers. Presnted at the 245th ACS National Meeting, New Orleans, LA, April 7−11, 2013, Abstract MEDI 8.
(46) Caldirola, P.; Johansson, G.; Nilsson, B. M.;2-, 3-, 4-, or 5-substituted-1-(benzenesulfonyl)indoles and their use in therapy. PCT Int. Appl. WO2002032863, 2002.
(47) Ramakrishna, N. V. S.; Kambhampati, R. S.; Deshpande, A. D.; Jasti, V. 4-(Heterocyclyl)alkyl-N-(arylsulfonyl)indole compounds and their use as 5-HT6 ligands and preparation. PCT Int. Appl. WO2008084491, 2008.
(48) Nirogi, R. V. S.; Badange, R.; Kambhampati, R.; Chindhe, A.; Deshpande, A. D.; Tiriveedhi, V.; Kandikere, V.; Muddana, N.; Abraham, R.; Khagga, M. Design, synthesis and pharmacological evaluation of 4-(piperazin-1-ylmethyl)-N1-arylsulfonyl indole derivatives as 5-HT6 receptor ligands. *Bioorg. Med. Chem. Lett.* **2012**, *22*, 7431−7435.
(49) ATCC (American Type Culture Collection) website, http://lgcstandards-atcc.org/
(50) Plowman, J.; Dykes, D. J.; Hollingshead, M.; Simpson-Herren, L.; Alley, M. C. Human tumor xenograft models in NCI drug development. *Anticancer Drug Development Guide: Preclinical Screening, Clinical Trials, and Approval*; Humana Press Inc.: Totowa, NJ, 1997; pp 101−125.
(51) Vonrhein, C.; Flensburg, C.; Keller, P.; Sharff, A.; Smart, O.; Paciorek, W.; Womack, T.; Bricogne, G. Data processing and analysis with the autoPROC toolbox. *Acta Crystallogr. D: Biol. Crystallogr.* **2011**, *67*, 293−302.
(52) Collaborative Computational Project, N.4. The CCP4 suite: programs for protein crystallography. *Acta Crystallogr. D: Biol. Crystallogr.* **1994**, *50*, 760−763.
(53) Bricogne, G. Ab initio macromolecular phasing: Blueprint for an expert system based on structure factor statistics with built-in stereochemistry. *Methods Enzymol.* **1997**, *277*, 14−18.
(54) Emsley, P.; Cowtan, K. Coot: Model-building tools for molecular graphics. *Acta Crystallogr. Sect. D: Biol. Crystallogr.* **2004**, *12*, 2126−2132.
(55) Evans, P. R. An introduction to data reduction: Space-group determination, scaling and intensity statistics. *Acta Crystallogr.* **2011**, *D67*, 282−292.